

# Implicit shock tracking for unsteady flows by the method of lines

A. Shi<sup>a,1,\*</sup>, P.-O. Persson<sup>a,b,2</sup>, M. J. Zahr<sup>c,3</sup>

<sup>a</sup>*Department of Mathematics, University of California, Berkeley, Berkeley, CA 94720, United States*

<sup>b</sup>*Mathematics Group, Lawrence Berkeley National Laboratory, 1 Cyclotron Road, Berkeley, CA 94720, United States*

<sup>c</sup>*Department of Aerospace and Mechanical Engineering, University of Notre Dame, Notre Dame, IN 46556, United States*

---

## Abstract

A recently developed high-order implicit shock tracking (HOIST) framework for resolving discontinuous solutions of inviscid, steady conservation laws [43, 45] is extended to the *unsteady* case. Central to the framework is an optimization problem which simultaneously computes a discontinuity-aligned mesh and the corresponding high-order approximation to the flow, which provides nonlinear stabilization and a high-order approximation to the solution. This work extends the implicit shock tracking framework to the case of unsteady conservation laws using a method of lines discretization via a diagonally implicit Runge-Kutta method by “solving a steady problem at each timestep”. We formulate and solve an optimization problem that produces a feature-aligned mesh and solution at each Runge-Kutta stage of each timestep, and advance this solution in time by standard Runge-Kutta update formulas. A Rankine-Hugoniot based prediction of the shock location together with a high-order, untangling mesh smoothing procedure provides a high-quality initial guess for the optimization problem at each time, which results in rapid convergence of the sequential quadratic programming (SQP) optimization solver. This method is shown to deliver highly accurate solutions on coarse, high-order discretizations without nonlinear stabilization and recover the design accuracy of the Runge-Kutta scheme. We demonstrate this framework on a series of inviscid, unsteady conservation laws in both one- and two- dimensions. We also verify that our method is able to recover the design order of accuracy of our time integrator in the presence of a strong discontinuity.

*Keywords:* shock tracking, shock fitting, method of lines, high-order methods, discontinuous Galerkin, high-speed flows

---

## 1. Introduction

It is widely believed that higher fidelity is required for problems with propagating waves, turbulent fluid flow, nonlinear interactions, and multiple scales [41]. This has resulted in a significant interest in high-order accurate methods, such as discontinuous Galerkin (DG) methods [8, 22], which have the potential to produce accurate solutions on coarse meshes. Among the most significant challenges associated with high-order methods is their sensitivity to under-resolved features, in particular for nonlinear problems where the spurious oscillations often cause a breakdown of the numerical solvers. This is exacerbated for problems with shocks where the low dissipation associated with high-order methods is insufficient to stabilize the solution. Since shocks are present in many important problems in fields such as aerospace, astrophysics, and combustion, this poses a fundamental barrier to widespread adoption of these methods.

Several approaches have been proposed to stabilize shocks, most of which are based on *shock capturing*, where the numerical discretization accounts for discontinuities independently of the computational grid. One simple method is to use a sensor that identifies the mesh elements in the shock region and reduce the degree of the approximating polynomial [3, 6]. A more sophisticated approach includes limiting, such as the weighted essentially non-oscillatory (WENO) schemes [20, 27, 23], which perform a high-order reconstruction near

---

\*Corresponding author

*Email addresses:* andrewshi94@berkeley.edu (A. Shi), persson@berkeley.edu (P.-O. Persson), mzahr@nd.edu (M. J. Zahr)

<sup>1</sup>Graduate student, Department of Mathematics, University of California, Berkeley

<sup>2</sup>Professor, Department of Mathematics, University of California, Berkeley

<sup>3</sup>Assistant Professor, Department of Aerospace and Mechanical Engineering, University of Notre Dame

discontinuities, but require a large computational stencil which offsets the attractive compactness properties of DG methods. For high-order methods, artificial viscosity has also proven to be competitive, since it can smoothly resolve the jumps in the solution without introducing additional discontinuities between the elements [31]. A recent comparative study of artificial viscosity models [42] discusses their relative merits, but notes they all suffer from a relatively strong dependency on a large number of empirical parameters which must be tuned. The main problem with all these approaches is they lead to globally first-order accurate schemes. This can be remedied by local mesh refinement around the shock ( $h$ -adaptivity) [13], although the anisotropic high-order mesh adaptation is challenging and requires highly refined elements near the shock. This issue is further complicated by transient problems where shocks and other local features propagate throughout the domain, requiring online adaptivity to be computationally feasible. Even with aggressive  $h$ - and  $p$ -adaptivity, simulations of complex, shock-dominated, unsteady flows are extremely challenging and expensive.

An alternative approach is *shock tracking* or *shock fitting*, where the computational mesh is moved such that its faces are aligned with the discontinuities in the solution. This is natural in the setting of a DG method since the numerical scheme already incorporates jumps between the elements and the approximate Riemann solvers employed on the element faces handle the discontinuities correctly. However, it is a difficult meshing problem since it essentially requires generating a fitted mesh to the (unknown) shock surface. Many previous approaches employ specialized formulations and solvers which are dimension dependent and do not easily generalize [21, 19, 4] and/or are limited to relatively simple problems [37, 38, 40]. In addition, early approaches to shock fitting have been applied to low-order schemes where the relative advantage over shock capturing is smaller than for high-order methods [39, 2]. One particular class of methods of note is *explicit* shock tracking, which is surveyed in [29, 34]. These strategies largely consist of explicitly identifying the shock and using the Rankine-Hugoniot conditions to compute its motion and states upstream and downstream of the shock. More recent developments in explicit shock tracking [32] use more sophisticated methods to compute shock velocities and discretize the flow equations, but ultimately still require a specialized strategy to explicitly track the shock separately from the remainder of the flow. These methods are not easily applicable to discontinuities whose topologies not known *a priori*. While interest in shock tracking/fitting methods has seen somewhat of a resurgence in recent years [7, 5, 18, 12], shock tracking is largely not used in practical CFD today.

In [43, 45], we introduced a novel approach to shock tracking for steady conservation laws that does not require explicitly generating a mesh of the unknown discontinuity surface. Rather, the conservation law is discretized on a mesh without knowledge of the discontinuity surface and an optimization problem is formulated such that its solution is the pair  $(\mathbf{u}, \mathbf{x})$ , where  $\mathbf{x}$  is the position of the mesh nodes that cause element faces to align with discontinuities in the flow and  $\mathbf{u}$  is the solution of discretized conservation law on the mesh defined by  $\mathbf{x}$ . That is, discontinuity tracking is implicitly achieved through the solution of an optimization problem and will be referred to as *implicit shock tracking*. While this approach works with any discretization that allows for inter-element discontinuities, we focus on high-order DG methods due to the high degree of accuracy attainable on coarse meshes, proper treatment of discontinuities with approximate Riemann solvers, and the ability to use curved elements to track discontinuities with curvature. The implicit tracking optimization problem proposed in [45] minimizes the violation of the DG residual in an enriched test space while enforcing that the standard DG (same test and trial space) equation is satisfied. This objective function is a surrogate for violation of the infinite-dimensional weak formulation of the conservation law, which endows the method with  $r$ -adaptive behavior: it promotes alignment of the mesh with discontinuities and adjusts nodes in smooth regions to improve approximation of the conservation law. The optimization problem is solved using a sequential quadratic programming method with a Levenberg-Marquardt Hessian approximation that simultaneously converges the mesh and solution to their optimal values, which never requires the fully converged DG solution on a non-aligned mesh and does not require nonlinear stabilization. The combination of implicit tracking with a DG discretization leads to a high-order accurate numerical method that has been shown to provide accurate approximations to high-speed inert [43, 45] and reacting flows [44].

In this work, we further extend the framework developed in [43, 45] for steady conservation laws (which can be applied to space-time formulations of unsteady conservation laws) to a method of lines discretization approach for unsteady problems. While space-time methods are attractive for a number of reasons, the method of lines approach tends to be more practical for complex problems when applicable, in large part

because computations are only required on a  $d$ -dimensional mesh instead of a time-coupled  $(d+1)$ -dimensional space-time mesh. The key ingredients of the method of lines approach are: 1) an Arbitrary Lagrangian-Eulerian formulation of the conservation law to handle the deforming mesh (which deforms to track the shock through the domain), 2) semi-discretization with DG to obtain a system of ordinary differential equations, 3) high-order temporal discretization with a diagonally implicit Runge-Kutta (DIRK) method, and 4) implicit shock tracking at each time step following the approach in [45]. We utilize a Rankine-Hugoniot-based procedure to predict the shock location at future times combined with a high-order mesh smoothing procedure with untangling capabilities to construct high quality initial guesses for the mesh and solution for the optimization problem at each time step. These initial guesses enhance the robustness of the method and significantly accelerate the performance of the optimization solver, to achieve rapid convergence.

To our knowledge, the only other approach to implicit shock tracking is the Moving Discontinuous Galerkin Method with Interface Condition Enforcement (MDG-ICE), proposed in [9, 11], where the authors enforce a DG discretization with unconventional numerical fluxes and the Rankine-Hugoniot interface conditions in a minimum-residual sense. In their approach, the interface condition is enforced along all faces of the mesh, separately from conservation law. Interestingly, enforcement of the interface condition circumvented traditional stability requirements for the DG numerical fluxes, allowing them to solely rely on fluxes interior to an element. Their method was shown to successfully track even complex discontinuity surfaces and provide high-order approximations to the conservation law on traditionally coarse, high-order meshes. In [10], they extended MDG-ICE to solve unsteady problems by space-time slab marching with a simplicial grid extrusion strategy. More recently, they extended MDG-ICE, originally developed for inviscid conservation laws, to viscous conservation laws [26] and reformulated it as a least-squares discontinuous Galerkin method [25], which endows the method with super-optimal convergence properties.

The remainder of this paper is organized as follows. Section 2 introduces the governing system of inviscid unsteady conservation laws, its spatial discretization using a DG method, and its temporal discretization using a diagonally implicit Runge-Kutta (DIRK) method. Section 3 presents the error-based objective function and the constrained optimization framework. Section 4 discusses practical details required for the proposed tracking framework such as initialization of the SQP solver. Finally, Section 5 presents a number of numerical experiments that demonstrate the method on a variety of unsteady flows using coarse, high-order meshes. We also demonstrate high-order temporal convergence of the method along with the rapid convergence of the SQP solver.

## 2. Governing equations and high-order numerical discretization

Consider a general system of  $m$  inviscid conservation laws, defined on the fixed domain  $\Omega \subset \mathbb{R}^d$  and subject to appropriate boundary conditions,

$$\frac{\partial U}{\partial t} + \nabla \cdot F(U) = 0 \quad \text{in } \Omega \times [0, T] \quad (1)$$

where  $U : \Omega \times [0, T] \rightarrow \mathbb{R}^m$  is the solution of the system of conservation laws,  $F : \mathbb{R}^m \rightarrow \mathbb{R}^{m \times d}$  is the flux function,  $\nabla := (\partial_{x_1}, \dots, \partial_{x_d})$  is the gradient operator in the physical domain such that  $\nabla W(x, t) = [\partial_{x_1} W(x, t) \quad \dots \quad \partial_{x_d} W(x, t)] \in \mathbb{R}^{N \times d}$  for any  $W : \Omega \times [0, T] \rightarrow \mathbb{R}^N$  and  $x \in \Omega$ ,  $t \in [0, T]$ , and the boundary of the domain  $\partial\Omega$  has outward unit normal  $n : \partial\Omega \rightarrow \mathbb{R}^d$ . The conservation law in (1) is supplemented with the initial condition  $U(x, 0) = \bar{U}(x)$  for all  $x \in \Omega$ , where  $\bar{U} : \Omega \rightarrow \mathbb{R}^m$ . In general, the solution  $U(x)$  may contain discontinuities, in which case, the conservation law (1) holds away from the discontinuities and the Rankine-Hugoniot conditions [28] hold at discontinuities.

Building on our previous work [43, 45], we will construct a high-order numerical method that tracks discontinuities with the computational grid as they evolve through the domain, which places three requirements on the discretization: 1) a high-order, stable, and convergent discretization of the conservation law in (1), 2) employs a solution basis that supports discontinuities between computational cells or elements, and 3) allows for deformation of the computational domain. As such, our method is based on a standard high-order DG-DIRK discretization of an Arbitrary Lagrangian-Eulerian (ALE) formulation of the governing equations. We insist on a high-order discretization given their proven ability [43, 9] to deliver accurate solutions on coarse discretizations provided discontinuities are tracked.

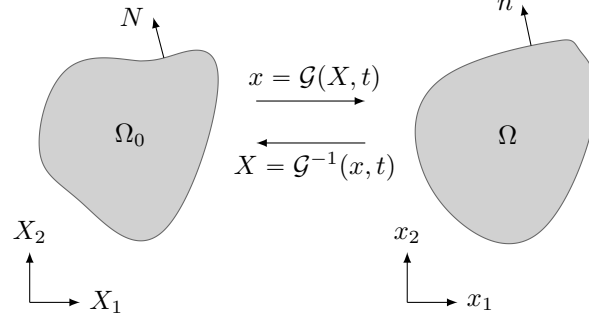


Figure 1: Mapping between reference and physical domains.

The remainder of this section will detail the discretization of the conservation law (1) using DG such that it reduces to the semi-discrete form

$$\mathbf{r}(\dot{\mathbf{u}}, \mathbf{u}, \dot{\mathbf{x}}, \mathbf{x}) = \mathbf{0} \quad (2)$$

where  $\mathbf{r} : \mathbb{R}^{N_u} \times \mathbb{R}^{N_u} \times \mathbb{R}^{N_x} \times \mathbb{R}^{N_x} \rightarrow \mathbb{R}^{N_u}$ ,  $\mathbf{u}$  is the semi-discrete representation of the conservation law state  $U$ , and  $\mathbf{x}$  is the semi-discrete representation of the conservation law domain  $\Omega$  (nodal coordinates of mesh nodes). We will then apply a high-order temporal discretization to (2) by a diagonally implicit Runge-Kutta method to yield a complete discretization of (1). The same discretization process can be used to yield a semi-discretization from an enriched *test* space and corresponding temporal discretization, which will be used in the definition of the proposed objective function.

### 2.1. Arbitrary Lagrangian-Eulerian formulation of conservation laws

We use an ALE formulation of the governing equations to account for the time-dependent domain deformations required to track discontinuities as they evolve. To this end, we introduce a time-dependent domain mapping (Fig. 1)

$$\mathcal{G} : \Omega_0 \times [0, T] \rightarrow \Omega; \quad \mathcal{G} : (X, t) \mapsto \mathcal{G}(X, t), \quad (3)$$

where  $\Omega_0 \subset \mathbb{R}^d$  is a fixed reference domain,  $T$  is the final time, and at each time  $t \in [0, T]$ ,  $\mathcal{G}(\cdot, t) : \Omega_0 \rightarrow \Omega$  is a diffeomorphism. We note that the domain  $\Omega$  is fixed, i.e.,  $\Omega$  occupies the same region of  $\mathbb{R}^d$  at any time  $t \in [0, T]$ ; the time-dependent diffeomorphism is introduced as an integral part of the proposed numerical method to track discontinuities as they evolve. Under the domain mapping (3), the conservation law (1) becomes

$$\frac{\partial U}{\partial t} + \nabla \cdot F(U) = 0 \quad \text{in } \mathcal{G}(\Omega_0, t) \quad (4)$$

Following the approach in [30], the conservation law on the physical domain  $\Omega$  is transformed to a conservation law on the reference domain  $\Omega_0$

$$\frac{\partial U_X}{\partial t} + \nabla_X \cdot F_X(U_X; G, v) = 0 \quad \text{in } \Omega_0 \quad (5)$$

where  $U_X : \Omega_0 \times [0, T] \rightarrow \mathbb{R}^m$  is the solution of the transformed conservation law,  $F_X : \mathbb{R}^m \times \mathbb{R}^{d \times d} \times \mathbb{R}^d \rightarrow \mathbb{R}^{m \times d}$  is the transformed flux function,  $\nabla_X := (\partial_{X_1}, \dots, \partial_{X_d})$  is the gradient operator on the reference domain, and the deformation gradient  $G : \Omega_0 \times [0, T] \rightarrow \mathbb{R}^{d \times d}$ , mapping Jacobian  $g : \Omega_0 \times [0, T] \rightarrow \mathbb{R}$ , and mapping velocity  $v : \Omega_0 \times [0, T] \rightarrow \mathbb{R}^d$  are defined as

$$G = \nabla_X \mathcal{G}, \quad g = \det G, \quad v = \frac{\partial \mathcal{G}}{\partial t}. \quad (6)$$

The transformed and physical solutions are related, for any  $X \in \Omega_0$  and  $t \in [0, T]$ , as

$$U_X(X, t) = g(X, t)U(\mathcal{G}(X, t), t) \quad (7)$$

and the transformed flux is defined as

$$F_X : (W_X; \Theta, \xi) \mapsto [(\det \Theta) F((\det \Theta)^{-1} W_X) - W_X \otimes \xi] \Theta^{-T}. \quad (8)$$

The unit normals in the reference and physical domain are related by

$$n = \frac{g G^{-T} N}{\|g G^{-T} N\|}. \quad (9)$$

The transformed conservation law is supplemented with the initial condition  $U_X(X, 0) = \bar{U}_X(X)$  for all  $X \in \Omega_0$ , where  $\bar{U}_X : \Omega_0 \rightarrow \mathbb{R}^m$  is  $\bar{U}_X(X) = g(X, 0) \bar{U}(\mathcal{G}(X, 0))$ . In this work, we take the reference domain to be the physical domain at time 0, which implies  $g(X, 0) = 1$ .

## 2.2. Discontinuous Galerkin discretization of the transformed conservation law

We use a nodal discontinuous Galerkin method [8, 22] to discretize the transformed conservation law (5). Let  $\mathcal{E}_h$  represent a discretization of the reference domain  $\Omega_0$  into non-overlapping, potentially curved, computational elements. The DG construction begins with the elementwise weak form of the conservation law (5) that results from multiplying each equation by a test function  $\psi_X$ , integrating over a single element  $K \in \mathcal{E}_h$ , and applying the divergence theorem

$$\int_K \psi_X \cdot \dot{U}_X dV + \int_{\partial K} \psi_X^+ \cdot F_X(U_X; G, v) N dS - \int_K F_X(U_X; G, v) : \nabla_X \psi_X dV = 0, \quad (10)$$

where  $N$  is the outward normal to the surface  $\partial K$  and  $\psi_X^+$  denotes the trace of  $\psi$  *interior* to element  $K$ . To ensure the face integrals are single-valued, we replace  $F_X(U_X; G, v) N$  in the second term with a numerical flux function  $\mathcal{H}_X : \mathbb{R}^m \times \mathbb{R}^m \times \mathbb{R}^d \times \mathbb{R}^{d \times d} \times \mathbb{R}^d \rightarrow \mathbb{R}^m$  associated with the reference inviscid flux  $F_X$

$$\int_K \psi_X \cdot \dot{U}_X dV + \int_{\partial K} \psi_X^+ \cdot \mathcal{H}_X(U_X^+, U_X^-, N; G, v) dS - \int_K F_X(U_X; G, v) : \nabla_X \psi_X dV = 0, \quad (11)$$

where  $U_X^+$  ( $U_X^-$ ) denotes the interior (exterior) trace of  $U_X$  to the element  $K$ ; for points  $X \in \partial K \cap \partial \Omega_0$ ,  $U_X^-$  is a boundary state constructed to enforce the appropriate boundary condition. In this work, we take the numerical flux to be a smoothed version of the Roe flux (Section 2.3). To establish the finite-dimensional (semi-discrete) form of (11), we introduce the DG approximation (trial) space of discontinuous piecewise polynomials associated with the mesh  $\mathcal{E}_h$

$$\mathcal{V}_h^p = \{v \in [L^2(\Omega_0 \times [0, T])]^m \mid v(\cdot, t)|_K \in [\mathcal{P}_p(K)]^m, \forall K \in \mathcal{E}_h, t \in [0, T]\} \quad (12)$$

where  $\mathcal{P}_p(K)$  is the space of polynomial functions of degree at most  $p \geq 1$  on the element  $K$ , and we take the DG test space to be  $\mathcal{V}_h^{p'}$ , where  $p' \geq p$ . We also define the space of admissible domain mappings as the space of continuous piecewise polynomials of degree  $q$  associated with the mesh  $\mathcal{E}_h$

$$\mathcal{W}_h = \{v \in [C^0(\Omega_0 \times [0, T])]^d \mid v(\cdot, t)|_K \in [\mathcal{P}_q(K)]^d, \forall K \in \mathcal{E}_h, t \in [0, T]\}. \quad (13)$$

We can now establish the finite dimensional form of (11) and the formal statement of DG as: given  $\mathcal{G}_h \in \mathcal{W}_h$ , find  $U_{X,h} \in \mathcal{V}_h^p$  such that for all  $\psi_{X,h} \in \mathcal{V}_h^{p'}$

$$\int_K \psi_{X,h} \cdot \dot{U}_{X,h} dV + \int_{\partial K} \psi_{X,h}^+ \cdot \mathcal{H}_X(U_{X,h}^+, U_{X,h}^-, N; G_h, v_h) dS - \int_K F_X(U_{X,h}; G_h, v_h) : \nabla_X \psi_{X,h} dV = 0, \quad (14)$$

where the DG residual form  $r_h^{p'p} : \mathcal{V}_h^{p'} \times \mathcal{V}_h^p \times \mathcal{W}_h \rightarrow \mathbb{R}$  is given by

$$r_h^{p',p} : (\psi_{X,h}, W_{X,h}, \mathcal{Q}_h) \mapsto \sum_{K \in \mathcal{E}_{h,q}} r_K^{p',p}(\psi_{X,h}, W_{X,h}, \mathcal{Q}_h), \quad (15)$$

and the elemental DG form  $r_K^{p',p} : \mathcal{V}_h^{p'} \times \mathcal{V}_h^p \times \mathcal{W}_h \rightarrow \mathbb{R}$  is given by

$$\begin{aligned} r_K^{p',p} : (\psi_{X,h}, W_{X,h}, \mathcal{Q}_h) \mapsto & \int_K \psi_{X,h} \cdot \dot{W}_{X,h} dV \\ & + \int_{\partial K} \psi_{X,h}^+ \cdot \mathcal{H}_X(W_{X,h}^+, W_{X,h}^-, N; \nabla_X \mathcal{Q}_h, \dot{\mathcal{Q}}_h) dS \\ & - \int_K F_X(W_{X,h}; \nabla_X \mathcal{Q}_h, \dot{\mathcal{Q}}_h) : \nabla_X \psi_{X,h} dV. \end{aligned} \quad (16)$$

Next, we introduce a (nodal) basis over each element for the test space ( $\mathcal{V}_h^p$ ), trial space ( $\mathcal{V}_h^{p'}$ ), and mapping space ( $\mathcal{W}_h$ ) to reduce (16) to a system of ordinary differential equations (ODEs) in residual form. In the case where  $p' = p$ , we denote the residual  $\mathbf{r} : \mathbb{R}^{N_u} \times \mathbb{R}^{N_u} \times \mathbb{R}^{N_x} \times \mathbb{R}^{N_x} \rightarrow \mathbb{R}^{N_u}$ , which is defined as

$$\mathbf{r} : (\dot{\mathbf{w}}, \mathbf{w}, \dot{\mathbf{y}}, \mathbf{y}) \mapsto \mathbf{m}\dot{\mathbf{w}} + \mathbf{f}(\mathbf{w}, \mathbf{y}, \dot{\mathbf{y}}), \quad (17)$$

where  $N_u = \dim \mathcal{V}_h^p$ ,  $N_x = \dim \mathcal{W}_h$ ,  $\mathbf{m} \in \mathbb{R}^{N_u \times N_u}$  is the mass matrix associated with the test/trial space  $\mathcal{V}_h^p$ , and  $\mathbf{f} : \mathbb{R}^{N_u} \times \mathbb{R}^{N_x} \times \mathbb{R}^{N_x} \rightarrow \mathbb{R}^{N_u}$  is the algebraic form of the second and third terms in (16). In this notation, the standard DG discretization reads: given  $\mathbf{x} : [0, T] \rightarrow \mathbb{R}^{N_x}$ , find  $\mathbf{u} : [0, T] \rightarrow \mathbb{R}^{N_u}$  such that

$$\mathbf{r}(\dot{\mathbf{u}}(t), \mathbf{u}(t), \dot{\mathbf{x}}(t), \mathbf{x}(t)) = \mathbf{0}, \quad \mathbf{u}(0) = \bar{\mathbf{u}}, \quad (18)$$

for all  $t \in [0, T]$ , where  $\mathbf{u}$  is the time-dependent coefficients of the DG solution,  $\mathbf{x}$  is the time-dependent coefficients of the domain mapping (nodal coordinates of the mesh), and  $\bar{\mathbf{u}} \in \mathbb{R}^{N_u}$  is the algebraic representation of the initial condition  $\bar{U}_X$ ; additionally, we define  $\bar{\mathbf{x}} \in \mathbb{R}^{N_x}$  as the initial condition for the nodal coordinates, i.e.,  $\bar{\mathbf{x}} = \mathbf{x}(0)$ . Typically, the evolution of the mesh coordinates  $\mathbf{x}(t)$  is known analytically or governed by a dynamical system (e.g., fluid-structure interaction); however, in this work, it will be determined as the solution of an optimization problem (after temporal discretization) such that discontinuities are tracked over time.

Finally, we use the expansions in the nodal bases to define the *enriched residual*  $\mathbf{R} : \mathbb{R}^{N_u} \times \mathbb{R}^{N_u} \times \mathbb{R}^{N_x} \times \mathbb{R}^{N_x} \rightarrow \mathbb{R}^{N'_u}$  associated with a trial space of degree  $p'$  as

$$\mathbf{R} : (\dot{\mathbf{w}}, \mathbf{w}, \dot{\mathbf{y}}, \mathbf{y}) \mapsto \mathbf{M}\dot{\mathbf{w}} + \mathbf{F}(\mathbf{w}, \mathbf{y}, \dot{\mathbf{y}}), \quad (19)$$

where  $N'_u = \dim \mathcal{V}_h^{p'}$ ,  $\mathbf{M} \in \mathbb{R}^{N'_u \times N_u}$  is the mass matrix associated with the test space  $\mathcal{V}_h^{p'}$  and trial space  $\mathcal{V}_h^p$ , and  $\mathbf{F} : \mathbb{R}^{N_u} \times \mathbb{R}^{N_x} \times \mathbb{R}^{N_x} \rightarrow \mathbb{R}^{N'_u}$  is the algebraic form of the second and third terms in (16). In this work, we take  $p' = p + 1$ , but other choices are possible as well. The enriched residual will be used in Section 3 to define the implicit tracking objective function.

### 2.3. Numerical flux function

The numerical flux function corresponding to the reference flux ( $\mathcal{H}_X$ , i.e. reference numerical flux) is a quantity that replaces the transformed flux dotted with the outward unit normal ( $F_X \cdot N$ ), as done from (10) to (11). It is given by

$$\mathcal{H}_X(U_X^+, U_X^-, N; G, v) = \|gG^{-T}N\| \tilde{\mathcal{H}}(U^+, U^-, n; v), \quad (20)$$

since by (7)-(9) we have

$$\mathcal{H}_X \sim F_X \cdot N = g(F - U \otimes v) \cdot G^{-T}N = \|gG^{-T}N\| (F - U \otimes v) \cdot n \sim \|gG^{-T}N\| \tilde{\mathcal{H}}, \quad (21)$$

where arguments have been dropped for brevity. Here,  $\tilde{\mathcal{H}} : \mathbb{R}^m \times \mathbb{R}^m \times \mathbb{R}^d \times \mathbb{R}^d \rightarrow \mathbb{R}^m$  is a modified numerical flux which corresponds to the modified flux function,  $\tilde{F} : \mathbb{R}^m \times \mathbb{R}^d \rightarrow \mathbb{R}^{m \times d}$ , which is related to the physical flux as

$$\tilde{F}(U; v) = F(U) - U \otimes v. \quad (22)$$



The modified flux accounts for the domain motion and is obtained from the numerical flux function corresponding to the physical flux,  $\mathcal{H} : \mathbb{R}^m \times \mathbb{R}^m \times \mathbb{R}^d \rightarrow \mathbb{R}^m$ . Notice that the Jacobian of the modified flux function only differs from the Jacobian of the physical flux by a scale multiple of the identity matrix (with scale factor  $v \cdot n$ ), which makes implementation of many numerical fluxes that depend on the eigenvalue decomposition of the Jacobian matrix, e.g., local Lax-Friedrichs, Roe, Vijayasundaram, straightforward given the decomposition of the Jacobian of the physical flux.

For example, consider linear advection of a scalar field  $U : \Omega \rightarrow \mathbb{R}$  in a spatially varying direction  $\beta : \Omega \rightarrow \mathbb{R}^d$  governed by a conservation law of the form (1) (see (53) in Section 5.1) with physical flux function

$$F_{\text{adv}}(U) = U\beta^T \quad (23)$$

with the corresponding upwind numerical flux

$$\mathcal{H}_{\text{up}}(U^+, U^-, n) = \begin{cases} (\beta \cdot n)U^+ & \text{if } \beta \cdot n \geq 0 \\ (\beta \cdot n)U^- & \text{if } \beta \cdot n < 0. \end{cases} \quad (24)$$

This can equivalently be written in terms of the absolute value function  $|\cdot| : \mathbb{R} \rightarrow \mathbb{R}_{\geq 0}$  as

$$\mathcal{H}_{\text{up}}(U^+, U^-, n) = 0.5 [(\beta \cdot n)(U^+ + U^-) + (U^+ - U^-)|\beta \cdot n|]. \quad (25)$$

Due to the linearity of the flux, the modified flux function is

$$\tilde{F}_{\text{adv}}(U) = U(\beta - v)^T, \quad (26)$$

which has an identical form as (23), albeit with a modified velocity field. Thus, the corresponding modified upwind numerical flux function is

$$\tilde{\mathcal{H}}_{\text{up}}(U^+, U^-, n; v) = 0.5 [((\beta - v) \cdot n)(U^+ + U^-) + (U^+ - U^-)|(\beta - v) \cdot n|]. \quad (27)$$

In [45], we showed that it is advantageous, in terms of solver performance, to have a numerical flux function that is smooth with respect to variations in the normal  $n$ . Following the approach in [45, 44], we introduce a smoothed version the upwind flux where the absolute value function is replaced with a smoothed absolute value function

$$\mathcal{H}_{\text{up}}^s(U^+, U^-, n) = 0.5 [(\beta \cdot n)(U^+ + U^-) + (U^+ - U^-)|\beta \cdot n|_s], \quad (28)$$

where  $|\cdot|_s : \mathbb{R} \rightarrow \mathbb{R}_{\geq 0}$  is a smooth approximation to the absolute value given by

$$|\cdot|_s : x \mapsto x \tanh(kx) \quad (29)$$

and  $k$  is a smoothness parameter (Fig. 2). In this work, we use  $k = 100$ . Previously, we had expressed numerical fluxes in terms of a smoothed Heaviside function, but we find the smoothed absolute value function performs better numerically as we are no longer smoothing a discontinuous function. Then, the smoothed version of the modified upwind numerical flux is given by

$$\tilde{\mathcal{H}}_{\text{up}}^s(U^+, U^-, n; v) = 0.5 [((\beta - v) \cdot n)(U^+ + U^-) + (U^+ - U^-)|(\beta - v) \cdot n|_s]. \quad (30)$$

Similarly, for the Euler equations, we use Roe's flux [33] with the absolute value of the eigenvalues replaced by the corresponding smoothed absolute value; a detailed derivation of the smoothed Roe flux for the reacting Euler equations (single reaction) is included in Appendix A of [44].

#### 2.4. High-order temporal discretization

Proceeding with the method of lines, we discretize the dynamical system in (18) using a diagonally implicit Runge-Kutta method (DIRK) to yield a sequence of algebraic systems of equations. Unlike fully implicit Runge-Kutta methods, an  $s$ -stage DIRK scheme has a Butcher tableau  $(A, b, c) \in \mathbb{R}^{s \times s} \times \mathbb{R}^s \times \mathbb{R}^s$  where  $A$  is lower triangular (Table 1). As a result, the  $i$ th stage only depends on the solution for stages  $1, \dots, i$ , allowing the stages to be solved sequentially. Because the nodal coordinates  $\mathbf{x}$  are unknown in the

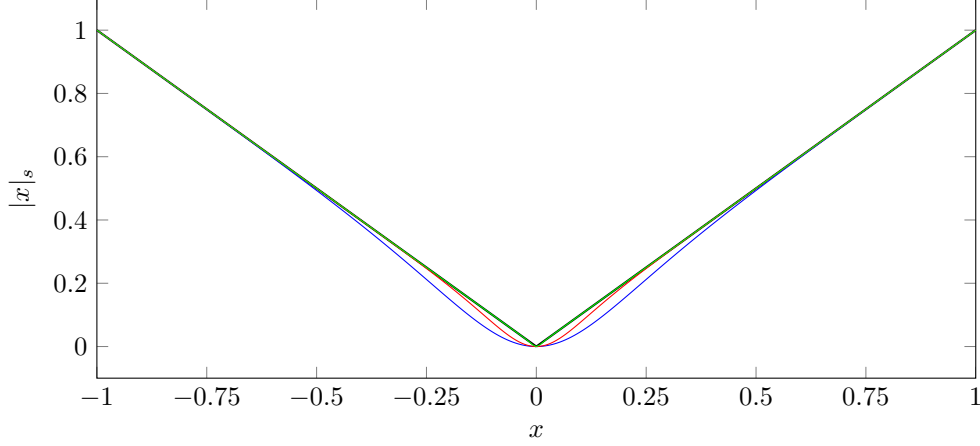


Figure 2: Smoothed absolute value function for  $k = 5$  (—),  $k = 10$  (—), and  $k = 100$  (—).  $k = \infty$  corresponds to the unsmoothed absolute value function (—).

Table 1: Butcher tableau for DIRK schemes

$$\begin{array}{c|c} \mathbf{c} & \mathbf{A} \\ \hline & \mathbf{b}^T \end{array} = \begin{array}{c|cc} c_1 & a_{11} & \\ \vdots & \vdots & \ddots \\ c_s & a_{s1} & \dots & a_{ss} \\ \hline & b_1 & \dots & b_s \end{array}$$

proposed setting, we first recast (18) as the following coupled system of ODEs

$$\begin{aligned} m\dot{\mathbf{u}}(t) + \mathbf{f}(\mathbf{u}(t), \mathbf{x}(t), \boldsymbol{\nu}(t)) &= \mathbf{0} \\ \dot{\mathbf{x}}(t) - \boldsymbol{\nu}(t) &= \mathbf{0} \\ \mathbf{u}(0) &= \bar{\mathbf{u}} \\ \mathbf{x}(0) &= \bar{\mathbf{x}} \end{aligned} \tag{31}$$

for  $t \in [0, T]$ , where  $\boldsymbol{\nu} : [0, T] \rightarrow \mathbb{R}^{N_x}$  is the unknown nodal velocity, defined as

$$\boldsymbol{\nu} : t \mapsto \dot{\mathbf{x}}(t). \tag{32}$$

Next, we partition the time interval  $[0, T]$  into  $N_T$  intervals of equal size  $\Delta t = T/N_T$  with endpoints  $\{t_n\}_{n=0}^{N_T}$ , where  $t_0 = 0$  and  $t_n = t_{n-1} + \Delta t$  for  $n = 1, \dots, N_T$ . In this setting, an  $s$ -stage DIRK discretization of (18) with Butcher tableau  $(A, b, c)$  reads: for  $n = 1, \dots, N_T$  and  $i = 1, \dots, s$ ,

$$\begin{aligned} \mathbf{u}_0 &= \bar{\mathbf{u}}, \quad \mathbf{u}_{n+1} = \mathbf{u}_n + \sum_{j=1}^s b_j \mathbf{k}_{n,j}^{\mathbf{u}}, \quad \mathbf{u}_{n,i} = \mathbf{u}_n + \sum_{j=1}^i a_{ij} \mathbf{k}_{n,j}^{\mathbf{u}} \\ \mathbf{x}_0 &= \bar{\mathbf{x}}, \quad \mathbf{x}_{n+1} = \mathbf{x}_n + \sum_{j=1}^s b_j \mathbf{k}_{n,j}^{\mathbf{x}}, \quad \mathbf{x}_{n,i} = \mathbf{x}_n + \sum_{j=1}^i a_{ij} \mathbf{k}_{n,j}^{\mathbf{x}} \\ m\mathbf{k}_{n,i}^{\mathbf{u}} &= -\Delta t \mathbf{f}(\mathbf{u}_{n,i}, \mathbf{x}_{n,i}, \boldsymbol{\nu}_{n,i}), \quad \mathbf{k}_{n,i}^{\mathbf{x}} = \Delta t \boldsymbol{\nu}_{n,i}, \quad \boldsymbol{\nu}_{n,i} = \boldsymbol{\nu}(t_n + c_i \Delta t) \end{aligned} \tag{33}$$

where  $\mathbf{u}_0, \mathbf{u}_n, \mathbf{u}_{n,i}, \mathbf{k}_{n,i}^{\mathbf{u}} \in \mathbb{R}^{N_u}$  and  $\mathbf{x}_0, \mathbf{x}_n, \mathbf{x}_{n,i}, \mathbf{k}_{n,i}^{\mathbf{x}}, \boldsymbol{\nu}_{n,i} \in \mathbb{R}^{N_x}$  are implicitly defined as the solution of (33);  $\mathbf{u}_n \approx \mathbf{u}(t_n)$  and  $\mathbf{x}_n \approx \mathbf{x}(t_n)$  are the state and mesh approximation at each time step  $n = 0, \dots, N_T$ ;  $\mathbf{u}_{n,i} \approx \mathbf{u}(t_n + c_i \Delta t)$  and  $\mathbf{x}_{n,i} \approx \mathbf{x}(t_n + c_i \Delta t)$  are the state and mesh approximations at each stage  $i = 1, \dots, s$  of each time interval  $n = 1, \dots, N_T$ ;  $\mathbf{k}_{n,i}^{\mathbf{u}}$  and  $\mathbf{k}_{n,i}^{\mathbf{x}}$  are the solution and mesh stage updates, and  $\boldsymbol{\nu}_{n,i} = \boldsymbol{\nu}(t_n + c_i \Delta t)$  is the mesh velocity. Because the mesh velocity  $\boldsymbol{\nu}$  is unknown, the system in (33) can neither be solved nor



evaluated in residual form.

Following the work in [15], we replace the unknown velocity function  $\boldsymbol{\nu}$  with a modified velocity function,  $\tilde{\boldsymbol{\nu}} : [0, T] \rightarrow \mathbb{R}^{N_{\mathbf{x}}}$ , that ensures the corresponding modified position  $\tilde{\mathbf{x}} : [0, T] \rightarrow \mathbb{R}^{N_{\mathbf{x}}}$ , defined as the solution of

$$\dot{\tilde{\mathbf{x}}}(t) - \tilde{\boldsymbol{\nu}}(t) = \mathbf{0}, \quad \tilde{\mathbf{x}}(0) = \bar{\mathbf{x}} \quad (34)$$

for  $t \in [0, T]$ , agree with the original stages  $\mathbf{x}_{n,i}$  when discretized with the same DIRK method. Discretization of (34) using the DIRK scheme reads: for  $n = 1, \dots, N_T$  and  $i = 1, \dots, s$ ,

$$\tilde{\mathbf{x}}_0 = \bar{\mathbf{x}}, \quad \tilde{\mathbf{x}}_{n+1} = \tilde{\mathbf{x}}_n + \sum_{j=1}^s b_i \tilde{\mathbf{k}}_{n,j}^{\mathbf{x}}, \quad \tilde{\mathbf{x}}_{n,i} = \tilde{\mathbf{x}}_n + \sum_{j=1}^i a_{ij} \tilde{\mathbf{k}}_{n,j}^{\mathbf{x}}, \quad \tilde{\mathbf{k}}_{n,i}^{\mathbf{x}} = \Delta t \tilde{\boldsymbol{\nu}}_{n,i}, \quad \tilde{\boldsymbol{\nu}}_{n,i} = \tilde{\boldsymbol{\nu}}(t_n + c_i \Delta t), \quad (35)$$

where  $\tilde{\mathbf{x}}_0, \tilde{\mathbf{x}}_n, \tilde{\mathbf{x}}_{n,i}, \tilde{\mathbf{k}}_{n,i}^{\mathbf{x}}, \tilde{\boldsymbol{\nu}}_{n,i} \in \mathbb{R}^{N_{\mathbf{x}}}$  are implicitly defined as the solution of (35);  $\tilde{\mathbf{x}}_n \approx \tilde{\mathbf{x}}(t_n)$  is the modified mesh approximation at each time step  $n = 0, \dots, T$ ;  $\tilde{\mathbf{x}}_{n,i} \approx \tilde{\mathbf{x}}(t_n + c_i \Delta t)$  is the modified mesh approximation at each stage  $i = 1, \dots, s$  of each time interval  $n = 1, \dots, T$ ;  $\tilde{\mathbf{k}}_{n,i}^{\mathbf{x}}$  is the modified mesh stage update, and  $\tilde{\boldsymbol{\nu}}_{n,i} = \tilde{\boldsymbol{\nu}}(t_n + c_i \Delta t)$  is the modified mesh velocity at each stage. Because the DIRK scheme only depends on the value of  $\tilde{\boldsymbol{\nu}}$  at  $t_n + c_i \Delta t$ , we only need to define its value at these points, i.e.,  $\tilde{\boldsymbol{\nu}}_{n,i}$ ; any smooth function  $\mathbf{z} : [0, T] \rightarrow \mathbb{R}^{N_{\mathbf{x}}}$  that satisfies  $\mathbf{z}(t_n + c_i \Delta t) = \tilde{\boldsymbol{\nu}}_{n,i}$  will lead to the same DIRK solution and is a valid choice for  $\tilde{\boldsymbol{\nu}}$ . The requirement that the modified and original mesh stages agree, i.e.,  $\tilde{\mathbf{x}}_{n,i} = \mathbf{x}_{n,i}$  for  $n = 1, \dots, N_T$  and  $i = 1, \dots, s$ , leads to

$$\mathbf{x}_{n,i} = \tilde{\mathbf{x}}_{n,i} = \tilde{\mathbf{x}}_n + \Delta t \sum_{j=1}^i a_{ij} \tilde{\boldsymbol{\nu}}_{n,j} = \mathbf{x}_n + \Delta t \sum_{j=1}^i a_{ij} \tilde{\boldsymbol{\nu}}_{n,j}, \quad (36)$$

where we used the definition of the stage  $\tilde{\mathbf{x}}_{n,i}$  in (35) and the relationship  $\tilde{\mathbf{x}}_n = \mathbf{x}_n$  for  $n = 0, \dots, N_T$ , which follows directly from the stage-consistent requirement ( $\tilde{\mathbf{x}}_{n,i} = \mathbf{x}_{n,i}$ ), the initial condition ( $\tilde{\mathbf{x}}_0 = \mathbf{x}_0 = \bar{\mathbf{x}}$ ), and that the DIRK schemes used to integrate (31) and (34) are the identical (same Butcher tableau). In the case where  $A$  is full rank, which is the case for fully and diagonally implicit Runge-Kutta methods, this equation can be inverted to express the modified velocity stages as a linear combination of the mesh stages

$$\tilde{\boldsymbol{\nu}}_{n,i} = \sum_{j=1}^i (\mathbf{A}^{-1})_{ij} \frac{\mathbf{x}_{n,j} - \mathbf{x}_n}{\Delta t}. \quad (37)$$

This approach leads to a *stage consistent* velocity approximation [15] in the sense that the modified velocity function is chosen such that it is consistent with the original mesh positions at each stage.

With the stage consistent mesh velocity approximation, the DIRK discretization in (33) becomes

$$\begin{aligned} \mathbf{u}_0 &= \bar{\mathbf{u}}, \quad \mathbf{u}_{n+1} = \mathbf{u}_n + \sum_{j=1}^s b_i \mathbf{k}_{n,j}^{\mathbf{u}}, \quad \mathbf{u}_{n,i} = \mathbf{u}_n + \sum_{j=1}^i a_{ij} \mathbf{k}_{n,j}^{\mathbf{u}} \\ \mathbf{x}_0 &= \bar{\mathbf{x}}, \quad \mathbf{x}_{n+1} = \mathbf{x}_n + \sum_{j=1}^s b_i \mathbf{k}_{n,j}^{\mathbf{x}}, \quad \mathbf{x}_{n,i} = \mathbf{x}_n + \sum_{j=1}^i a_{ij} \mathbf{k}_{n,j}^{\mathbf{x}} \\ m \mathbf{k}_{n,i}^{\mathbf{u}} &= -\Delta t \mathbf{f}(\mathbf{u}_{n,i}, \mathbf{x}_{n,i}, \tilde{\boldsymbol{\nu}}_{n,i}), \quad \mathbf{k}_{n,i}^{\mathbf{x}} = \Delta t \tilde{\boldsymbol{\nu}}_{n,i} \end{aligned} \quad (38)$$

for  $n = 1, \dots, N_T$  and  $i = 1, \dots, s$ , where the stage velocity is defined in (37). Even though the unknown velocity function has been eliminated using the stage consistent velocity approximation, the new system (38) is underdetermined because there are effectively  $N_{\mathbf{u}}$  equations in  $N_{\mathbf{u}} + N_{\mathbf{x}}$  unknowns at a fixed stage. This will be resolved by the optimization-based tracking formulation in the next section.

To close this section, we convert the modified DIRK system in (38) to residual form  $\mathbf{r}_{n,i} : \mathbb{R}^{N_{\mathbf{u}}} \times \mathbb{R}^{N_{\mathbf{x}}} \rightarrow \mathbb{R}^{N_{\mathbf{u}}}$  at a fixed step  $n \in \{1, \dots, N_T\}$  and stage  $i \in \{1, \dots, s\}$  as

$$\mathbf{r}_{n,i} : (\mathbf{w}, \mathbf{y}) \mapsto m \boldsymbol{\xi}_{n,i}(\mathbf{w}) + \Delta t \mathbf{f}(\mathbf{w}, \mathbf{y}, \boldsymbol{\zeta}_{n,i}(\mathbf{y})), \quad (39)$$

Table 2: Butcher tableau for DIRK1 (*left*), DIRK2 (*middle*), and DIRK3 (*right*), where  $\alpha = 1 - \frac{1}{\sqrt{2}}$ ,  $\beta = 0.435866521508459$ ,  $\gamma = -\frac{6\beta^2-16\beta+1}{4}$ , and  $\omega = \frac{6\beta^2-20\beta+5}{4}$ .

$$\begin{array}{c|c} 1 & 1 \\ \hline & 1 \end{array} \qquad \begin{array}{c|cc} \alpha & \alpha & 0 \\ 1 & 1-\alpha & \alpha \\ \hline & 1-\alpha & \alpha \end{array} \qquad \begin{array}{c|ccc} \beta & & & \\ \frac{1+\beta}{2} & \frac{1+\beta}{2}-\beta & \beta & \\ \hline \gamma + \omega + \beta & \gamma & \omega & \beta \\ & \gamma & \omega & \beta \end{array}$$

where  $\xi_{n,i} : \mathbb{R}^{N_u} \rightarrow \mathbb{R}^{N_u}$  maps the state stage ( $\mathbf{u}_{n,i}$ ) to the corresponding stage update ( $\mathbf{k}_{n,i}^u$ )

$$\xi_{n,i} : \mathbf{w} \mapsto (A^{-1})_{ii}(\mathbf{w} - \mathbf{u}_n) + \sum_{j=1}^{i-1} (A^{-1})_{ij}(\mathbf{u}_{n,j} - \mathbf{u}_n) \quad (40)$$

and  $\zeta_{n,i} : \mathbb{R}^{N_x} \rightarrow \mathbb{R}^{N_x}$  maps the mesh stage ( $\mathbf{x}_{n,i}$ ) to the corresponding stage-consistent velocity ( $\tilde{\mathbf{v}}_{n,i}$ ) as

$$\zeta_{n,i} : \mathbf{y} \mapsto (A^{-1})_{ii} \frac{\mathbf{y} - \mathbf{x}_n}{\Delta t} + \sum_{j=1}^{i-1} (A^{-1})_{ij} \frac{\mathbf{x}_{n,j} - \mathbf{x}_n}{\Delta t}. \quad (41)$$

Similarly, we define the corresponding fully discrete enriched residual function  $\mathbf{R}_{n,i} : \mathbb{R}^{N_u} \times \mathbb{R}^{N_x} \rightarrow \mathbb{R}^{N'_u}$  as

$$\mathbf{R}_{n,i} : (\mathbf{w}, \mathbf{y}) \mapsto M\xi_{n,i}(\mathbf{w}) + \Delta t \mathbf{F}(\mathbf{w}, \mathbf{y}, \zeta_{n,i}(\mathbf{y})), \quad (42)$$

which we use in next section to define the objective function of the implicit tracking optimization problem. Notice that for  $\mathbf{R}_{n,i}$  only the *spatial* test space is enriched; the temporal discretization in  $\mathbf{r}_{n,i}$  and  $\mathbf{R}_{n,i}$  is identical.

In this work, we consider three  $L$ -stable DIRK schemes with order of accuracy equal to the number of stages  $s$ ; Butcher tableaus given in Table 2. We denote the  $k$ -th order accurate DIRK scheme as DIRK $k$ , i.e. 1st order DIRK is DIRK1, etc. We note that DIRK1 is equivalent to the Backward Euler scheme.

### 3. Optimization formulation of $r$ -adaptivity for implicit tracking of discontinuities

In this section, we extend the high-order implicit shock tracking framework from [43, 45] to time-dependent problems using a method of lines approach (in contrast to the space-time approach in [9, 45]). Following the approach in [45], we recast the fully discrete conservation law as a PDE-constrained optimization problem over the discrete solution and mesh that aims to align element faces with discontinuities at each Runge-Kutta stage for every timestep. We also review the associated SQP solver for this optimization problem developed in [45].

#### 3.1. Constrained optimization formulation

We formulate the problem of tracking discontinuities at a given stage  $i$  and timestep  $n$  as a constrained optimization problem over the PDE state and mesh stage that minimizes an objective function,  $f_{n,i} : \mathbb{R}^{N_u} \times \mathbb{R}^{N_x} \rightarrow \mathbb{R}$ , while enforcing the DG-DIRK discretization. That is, we define  $\mathbf{u}_{n,i} \in \mathbb{R}^{N_u}$  and  $\mathbf{x}_{n,i} \in \mathbb{R}^{N_x}$  as

$$(\mathbf{u}_{n,i}, \mathbf{x}_{n,i}) := \arg \min_{\mathbf{w} \in \mathbb{R}^{N_u}, \mathbf{y} \in \mathbb{R}^{N_x}} f_{n,i}(\mathbf{w}, \mathbf{y}) \quad \text{subject to: } \mathbf{r}_{n,i}(\mathbf{w}, \mathbf{y}) = \mathbf{0}. \quad (43)$$

for  $n = 1, \dots, N_T$  and  $i = 1, \dots, s$ . For a fixed time step  $n$ , once the stage states  $\{\mathbf{u}_{n,i}\}_{i=1}^s$  and meshes  $\{\mathbf{x}_{n,i}\}_{i=1}^s$  are computed, the state and mesh can be advanced to the next time step ( $\mathbf{u}_{n+1}$  and  $\mathbf{x}_{n+1}$ ) using the relationships in (38). The DIRK schemes considered in this work (Table 2) satisfy the property that  $A_{si} = b_i$  for  $i = 1, \dots, s$ , which implies the state and mesh at the final stage of time step  $n$  are identical to the state and mesh at time step  $n+1$ , i.e.,  $\mathbf{u}_{n+1} = \mathbf{u}_{n,s}$  and  $\mathbf{x}_{n+1} = \mathbf{x}_{n,s}$ .

The objective function is constructed such that the solution of the PDE-constrained optimization problem is a feature-aligned mesh by using the norm of the enriched DG-DIRK residual

$$f_{n,i} : (\mathbf{w}, \mathbf{y}) \mapsto \frac{1}{2} \|\mathbf{R}_{n,i}(\mathbf{w}, \mathbf{y})\|_2^2. \quad (44)$$

This follows on a large body of work that uses residual-based error indicators to drive  $h$ -,  $p$ -, and  $r$ -adaptivity [14]. This is the same objective function used in our previous work for steady conservation laws, where it was shown to lead to a robust and reliable tracking framework; for details, see [45].

Unlike the steady case discussed in [45], we do not include the mesh quality term in the objective function for the unsteady (method of lines) case. In the steady case, there is no information about the shock location *a priori*, which usually requires significant deformation to the initial mesh to align with shocks, necessitating the use of a mesh regularization term in the objective function. However, in the context of timestepping, we have useful information from the previous timestep to use as an initial guess for both the state and mesh. We can combine this information along with the Rankine-Hugoniot conditions and a high-order mesh smoothing procedure to obtain an excellent initial guess for the mesh at each Runge-Kutta stage (Section 4). In a sense, the additional time dimension allows the mesh regularization to be decoupled from the implicit shock tracking procedure, which is one advantage of the method of lines discretization over the space-time formulation for solving unsteady problems.

### 3.2. SQP solver for optimization-based discontinuity tracking

The Lagrangian of the optimization problem in (43)  $\mathcal{L} : \mathbb{R}^{N_u} \times \mathbb{R}^{N_x} \times \mathbb{R}^{N_u} \rightarrow \mathbb{R}$  takes the form

$$\mathcal{L}(\mathbf{u}, \mathbf{x}, \boldsymbol{\lambda}) = f(\mathbf{u}, \mathbf{x}) - \boldsymbol{\lambda}^T \mathbf{r}(\mathbf{u}, \mathbf{x}), \quad (45)$$

where  $\boldsymbol{\lambda} \in \mathbb{R}^{N_u}$  is a vector of Lagrange multipliers associated with the DG constraint in (43). We drop all the subscripts in this section for brevity. The first-order optimality, or Karush-Kuhn-Tucker (KKT), conditions state that the  $(\mathbf{u}^*, \mathbf{x}^*)$  is a first-order solution of the optimization problem if there exists  $\boldsymbol{\lambda}^*$  such that

$$\frac{\partial f}{\partial \mathbf{u}}(\mathbf{u}^*, \mathbf{x}^*)^T - \frac{\partial \mathbf{r}}{\partial \mathbf{u}}(\mathbf{u}^*, \mathbf{x}^*)^T \boldsymbol{\lambda}^* = \mathbf{0}, \quad \frac{\partial f}{\partial \mathbf{x}}(\mathbf{u}^*, \mathbf{x}^*)^T - \frac{\partial \mathbf{r}}{\partial \mathbf{x}}(\mathbf{u}^*, \mathbf{x}^*)^T \boldsymbol{\lambda}^* = \mathbf{0}, \quad \mathbf{r}(\mathbf{u}^*, \mathbf{x}^*) = \mathbf{0}. \quad (46)$$

Since the DG Jacobian with respect to the state variables  $\mathbf{u}$  is assumed to be invertible, we define the estimate of the optimal Lagrange multiplier  $\hat{\boldsymbol{\lambda}} : \mathbb{R}^{N_u} \times \mathbb{R}^{N_x} \rightarrow \mathbb{R}^{N_u}$  such that the first equation ( $\nabla_{\mathbf{u}} \mathcal{L} = 0$ ) (adjoint equation) is always satisfied

$$\hat{\boldsymbol{\lambda}}(\mathbf{u}, \mathbf{x}) = \frac{\partial \mathbf{r}}{\partial \mathbf{u}}(\mathbf{u}, \mathbf{x})^{-T} \frac{\partial f}{\partial \mathbf{u}}(\mathbf{u}, \mathbf{x})^T. \quad (47)$$

Then the optimality criteria becomes

$$\mathbf{c}(\mathbf{u}^*, \mathbf{x}^*) := \frac{\partial f}{\partial \mathbf{x}}(\mathbf{u}^*, \mathbf{x}^*)^T - \frac{\partial \mathbf{r}}{\partial \mathbf{x}}(\mathbf{u}^*, \mathbf{x}^*)^T \frac{\partial \mathbf{r}^*}{\partial \mathbf{u}^*}(\mathbf{u}^*, \mathbf{x}^*)^{-T} \frac{\partial f}{\partial \mathbf{u}^*}(\mathbf{u}^*, \mathbf{x}^*)^T = \mathbf{0}, \quad \mathbf{r}(\mathbf{u}^*, \mathbf{x}^*) = \mathbf{0} \quad (48)$$

Because the optimization problem (43) *exactly matches the form* of the optimization problem for the steady case [45], we use the same SQP solver that defines the sequences  $\{\mathbf{u}^{(k)}\}_{k=0}^{\infty} \subset \mathbb{R}^{N_u}$  and  $\{\mathbf{x}^{(k)}\}_{k=0}^{\infty} \subset \mathbb{R}^{N_x}$  as

$$\mathbf{u}^{(k+1)} = \mathbf{u}^{(k)} + \alpha_{k+1} \Delta \mathbf{u}^{(k+1)}, \quad \mathbf{x}^{(k+1)} = \mathbf{x}^{(k)} + \alpha_{k+1} \Delta \mathbf{x}^{(k+1)}, \quad (49)$$

for  $k = 0, 1, \dots$ , where  $\alpha_{k+1} \in (0, 1]$  is a step length which can be determined by a line search procedure, and  $\Delta \mathbf{u}^{(k+1)} \in \mathbb{R}^{N_u}$  and  $\Delta \mathbf{x}^{(k+1)} \in \mathbb{R}^{N_x}$  are search directions. At a given iteration  $k$ , the search directions  $\Delta \mathbf{u}^{(k)}$  and  $\Delta \mathbf{x}^{(k)}$  are computed simultaneously as the solution of a quadratic approximation to the optimization problem in (43) with a regularized Levenberg-Marquardt approximation of the Hessian; for details, see [45]. A pair  $(\mathbf{u}, \mathbf{x})$  is considered a solution of (43) if  $\|\mathbf{c}(\mathbf{u}, \mathbf{x})\| < \epsilon_1$  and  $\|\mathbf{r}(\mathbf{u}, \mathbf{x})\| < \epsilon_2$  for tolerances  $\epsilon_1, \epsilon_2 > 0$ .

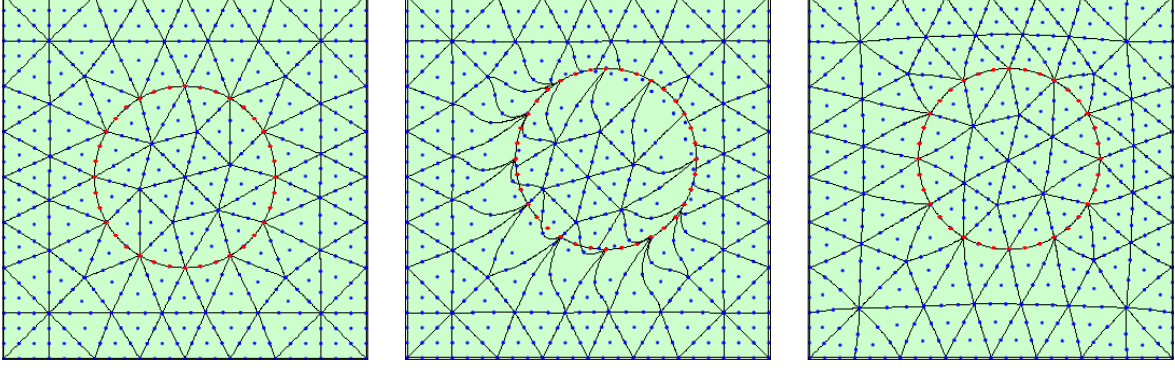


Figure 3: Shock nodes (.....) (left), advected by instantaneous shock speed (middle) and smoothed mesh (right).

## 4. Practical considerations

### 4.1. Initial guess for optimization

The implicit shock tracking optimization problem (43) is non-convex and therefore the initial guess for the SQP solver is critical to obtain a good solution. In the method of lines setting where implicit shock tracking is performed at each time step, an obvious idea for the initial guess is the converged mesh and solution from the previous time  $t_n$ . In practice, this is too far off to attain good convergence properties except for prohibitively small choices of timestep  $\Delta t$ . Instead, we employ an initial guess where we advect each node on the discontinuity surface from the previous time by the instantaneous shock speed determined by the Rankine-Hugoniot conditions (Fig. 3). The remaining nodes are updated using a standard optimization-based mesh smoothing using the high-order mesh distortion metric  $r_K^{\text{msh}} : \mathcal{W}_h \rightarrow \mathbb{R}$  developed in [17], defined as

$$r_{\text{msh}}^K : \mathcal{Q} \mapsto \int_K \left( \frac{\|\nabla_X \mathcal{Q}\|_F^2}{d(\det \nabla_X \mathcal{Q})_+^{2/d}} \right)^2 dv. \quad (50)$$

This provides a good initial guess for the shock-aligned mesh for each stage of the optimization problem. However, the advection of these shock nodes can result in a tangled mesh (Fig. 3, middle). We modify the mesh distortion metric (50) following the approach in [16] where the Jacobian ( $\det \nabla_X \mathcal{Q}$ ) is regularized to allow for the optimization procedure to recover from initially invalid configurations.

For the initial guess for the solution, we use the converged physical solution ( $U$ ) from the previous timestep. However, since we applied our DG discretization to the transformed reference conservation law (5), we are solving for the reference solution ( $U_X$ ). Therefore, to use the physical solution at time  $t_n$  as the initial guess for time  $t_{n+1}$ , we multiply it by the ratio of the Jacobian of the initial guess for the mapping at time  $t_{n+1}$  (advection based on Rankine-Hugoniot conditions and smoothing) to the Jacobian of the converged mapping at time  $t_n$ . More precisely, the initial guess for the  $i$ th Runge-Kutta stage in *physical* space, denoted  $\check{U}_h$ , is obtained by constant extrapolation of the physical state at time  $t$

$$\check{U}_h(x, t + c_i \Delta t) := U_h(x, t) = g_h(X, t)^{-1} U_{X_h}(X, t). \quad (51)$$

Let  $\tilde{\mathcal{G}} \in \mathcal{W}_h$  be the mapping to the configuration obtained by the Rankine-Hugoniot-based procedure and associated smoothing, then the initial guess for the  $i$ th Runge-Kutta stage in the *reference* domain, denoted  $\check{U}_{X_h}$ , is

$$\check{U}_{X_h}(X, t + c_i \Delta t) := \tilde{g}(X, t + c_i \Delta t) \check{U}_h(x, t + c_i \Delta t) = \frac{\tilde{g}(X, t + c_i \Delta t)}{g_h(X, t)} U_{X_h}(X, t). \quad (52)$$

Future work to enhance the robustness of these initial guesses might consider more advanced methods to approximate the shock velocity [32] and higher order extrapolation-based estimates for the solution.

### 4.2. Line search

In the steady case, the initial mesh is generated independently of the *a priori* unknown shock location, and as such can begin quite far from alignment with the shock. Element collapses were required to remove

small and poorly shaped elements that arose between iterations as the coarse high-order mesh deformed to align with the shock. Because of this, we chose the step length parameter  $\alpha_{k+1}$  of (49) based off a backtracking line search procedure based on the  $\ell_1$  merit function in our previous work [45].

In this work, we simply take  $\alpha_k = 1$  and do not require any topology changes to the mesh. This is possible because we are able to construct high-quality initial guesses for the optimization problem in the unsteady case that already contain information about the shock (unlike the steady case). In Section 5, we demonstrate this choice leads to **rapid convergence** of the SQP solver.

## 5. Numerical experiments

In this section, we introduce three inviscid unsteady conservation laws and demonstrate the tracking framework on five problems with discontinuous solutions of varying difficulty. We also demonstrate high-order convergence in time and present the convergence behavior of the SQP solver.

### 5.1. Linear advection

The first problem we consider is linear advection of a scalar quantity  $U$  through a domain  $\Omega \subset \mathbb{R}^d$

$$\begin{aligned} \frac{\partial}{\partial t} U(x, t) + \frac{\partial}{\partial x_j} (U(x, t) \beta_j(x)) &= 0 \quad \text{for } x \in \Omega, \ t \in [0, T] \\ U(x, 0) &= \bar{U}(x) \quad \text{for } x \in \Omega, \end{aligned} \quad (53)$$

where  $U : \Omega \times [0, T] \rightarrow \mathbb{R}$  is the conserved quantity implicitly defined as the solution of (53),  $\beta : \Omega \rightarrow \mathbb{R}^d$  is the flow direction, and  $\bar{U} : \Omega \rightarrow \mathbb{R}$  is the initial condition.

#### 5.1.1. 1D spatially varying advection

As a simple benchmark problem to demonstrate the capabilities and performance of the unsteady shock tracking framework, we consider the advection equation in one spatial dimension with a spatially varying advection field  $\beta : \Omega \rightarrow \mathbb{R}$

$$\beta : x \mapsto 1 + \frac{1}{2} \sin^2(2\pi x) \quad (54)$$

with initial condition  $\bar{U} : \Omega \rightarrow \mathbb{R}$ :

$$\bar{U}(x) = \begin{cases} \sin(\pi x) & x \leq 0.5 \\ \sin(\pi(x - 1)) & x > 0.5 \end{cases} \quad (55)$$

and periodic boundary conditions. We initialize with a mesh of the reference domain  $\Omega_0 = [0, 1]$ , which we construct such that an element interface lies at the initial shock location ( $x = 0.5$ ), i.e., the shock in the initial condition is tracked. The shock tracking solution is computed using a DG discretization on this equispaced mesh with 20 elements of degree  $p = 4$ ,  $q = 1$  and a DIRK3 temporal discretization with 25 time steps with final time  $T = 0.25$  (Figure 4). The SQP solver is used with tolerances  $\epsilon_1 = 10^{-6}$  and  $\epsilon_2 = 10^{-8}$ . At each timestep  $n + 1$ , we are able to obtain a solution to within the specified tolerances, which corresponds to the solution of the optimization problem (43) at time step  $n$  and stage  $s$ , and only need 2-3 iterations of the SQP solver to do so (Figure 5). Note that the  $s$ th stage tends to be more difficult for the SQP solver – one possible explanation is because each stage of the DIRK method has low stage order (first order), making it easier on the SQP solver compared to the  $s$ th stage, which is in fact the high-order solution because of our specific choice of DIRK schemes. We acknowledge this is an easy example for the SQP solver, and will demonstrate similar behavior for a more challenging example in the following sections.

We obtain a reference solution of (53) at  $T = 0.25$  using the method of characteristics; the characteristic equations and corresponding solution are integrated using classical RK4 with 10,000 timesteps. The shock tracking solution compares well to the reference solution at the final time  $T = 0.25$  (Figure 6). We use this reference solution to demonstrate high-order convergence in time of both the  $L^1$  error of the solution at the final time and the shock location, verifying the design order of accuracy of the DIRK $k$  schemes even in the presence of a discontinuity (Figure 7).

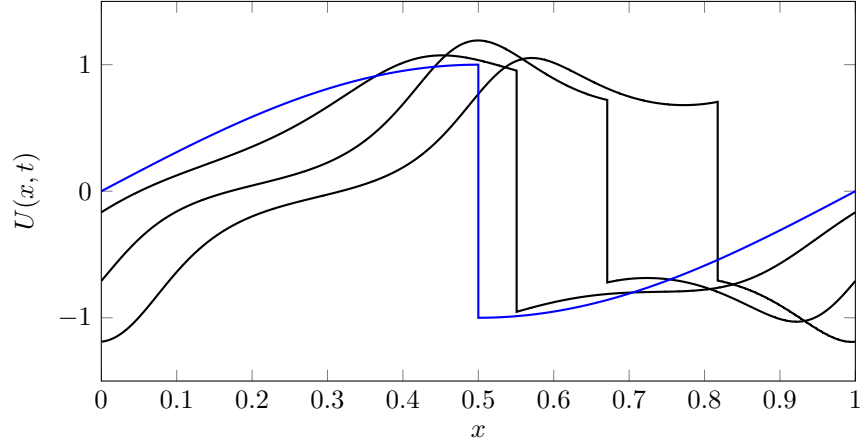


Figure 4: Method of lines solution of the one-dimensional, spatially varying advection equation with  $p = 4, q = 1$ . Initial condition  $\bar{U}(x)$  (—) and tracking solution at times  $t = 0.05, 0.15, 0.25$  (—).

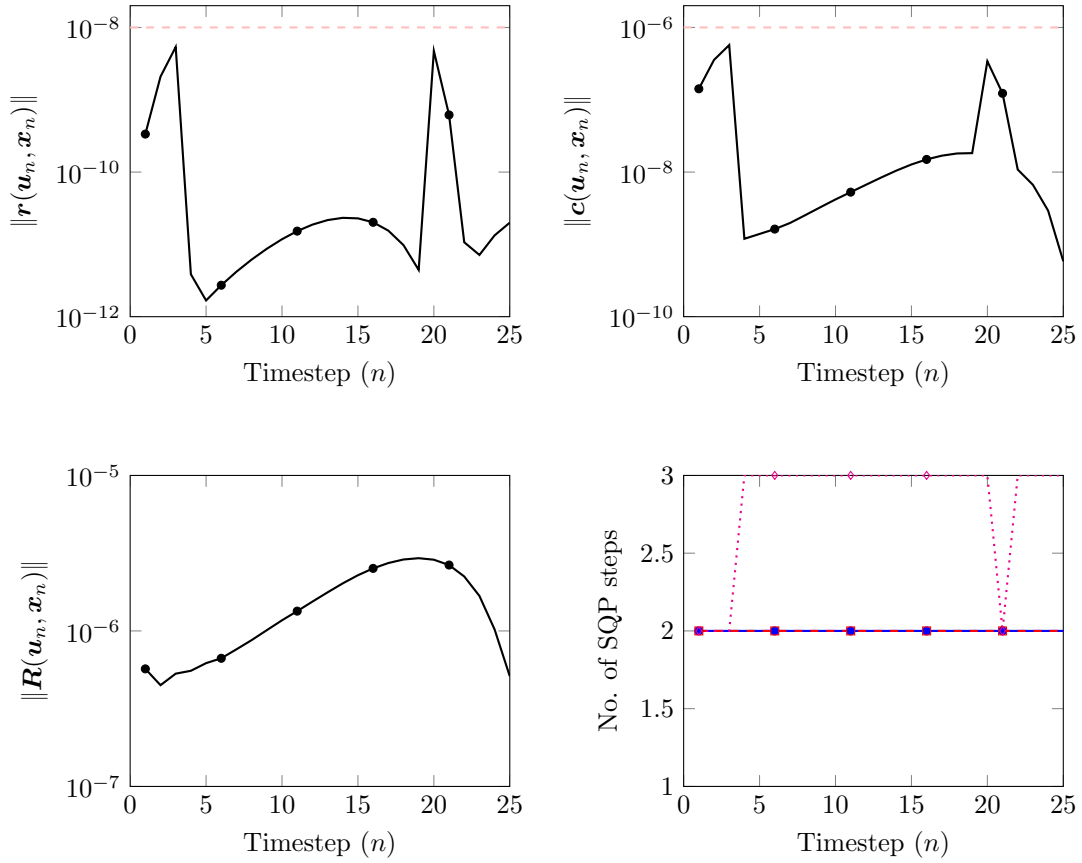


Figure 5: Final converged value of the constraint (*top left*), optimality condition (*top right*), and objective function (*bottom left*) for the solution to 1D spatially varying advection at each timestep (—) and the specified tolerances (---), and the number of SQP steps needed at each stage of each time step for convergence (*bottom right*); stage 1: (—), stage 2 (—), stage 3 (—).

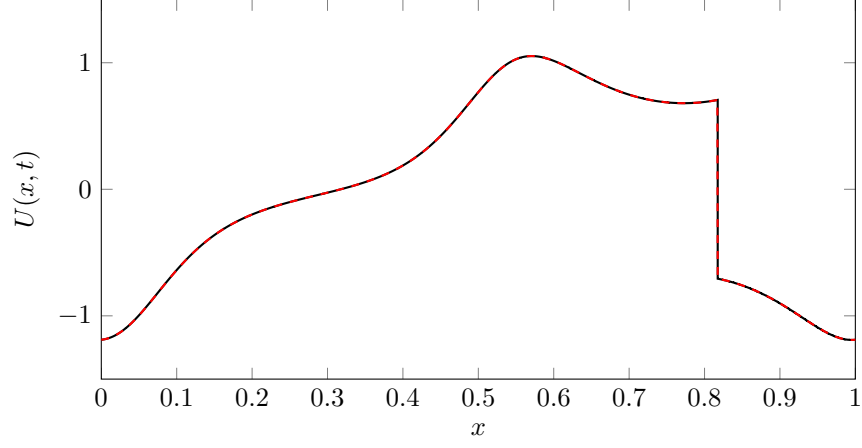


Figure 6: Comparison of shock tracking (—) and reference (---) solutions at  $T = 0.25$ .

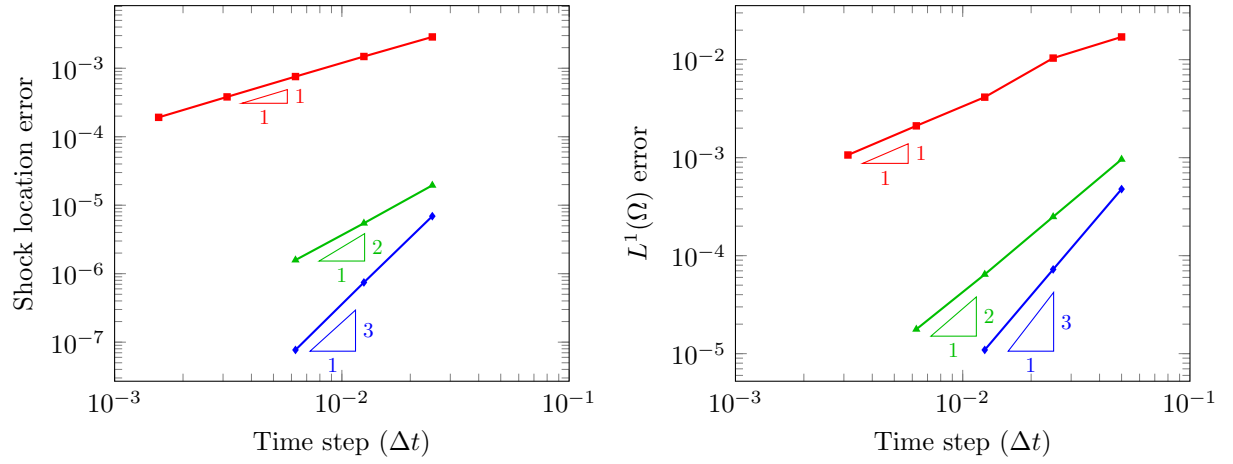


Figure 7: Temporal convergence of the DIRK1 (—■—), DIRK2 (—▲—), and DIRK3 (—◆—) schemes for the  $L^1$  error of the shock location (*left*) and the solution (*right*) for the spatially varying advection equation.



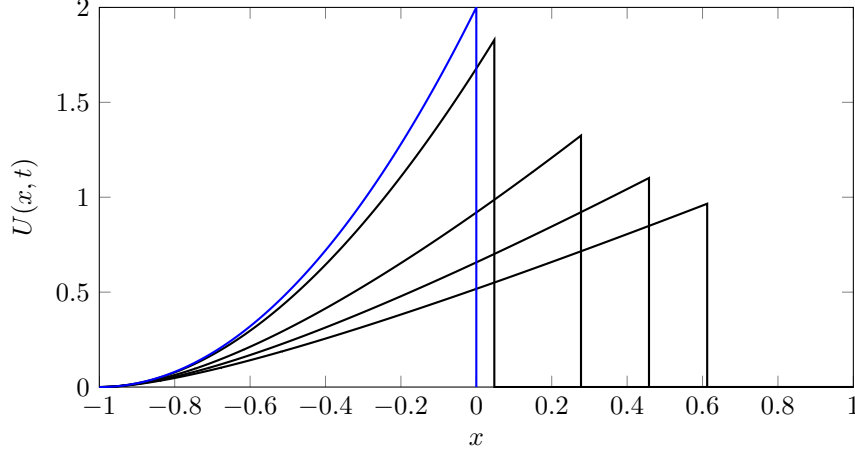


Figure 8: Method of lines solution of the one-dimensional, inviscid Burgers' equation with  $p = 4, q = 1$ , including initial condition  $\bar{U}(x)$  (—) and tracking solution at times  $t = 0.05, 0.35, 0.65, 0.95$  (—).

### 5.2. Time-dependent, inviscid Burgers' equation

The time-dependent, inviscid Burgers' equation governs nonlinear advection of a scalar quantity through the domain  $\Omega \subset \mathbb{R}^d$

$$\begin{aligned} \frac{\partial}{\partial t} U(x, t) + \frac{\partial}{\partial x_j} \left( \frac{1}{2} U(x, t)^2 \beta_j \right) &= 0 & \text{for } x \in \Omega, \ t \in [0, T] \\ U(x, t) &= 0 & \text{for } x \in \partial\Omega, \ t \in [0, T] \\ U(x, 0) &= \bar{U}(x) & \text{for } x \in \Omega, \end{aligned} \quad (56)$$

where  $U : \Omega \times [0, T] \rightarrow \mathbb{R}$  is the conserved quantity implicitly defined as the solution of (56),  $\beta \in \mathbb{R}^d$  is the flow direction, and  $\bar{U} : \Omega \rightarrow \mathbb{R}$  is the initial condition. We investigate this problem in both one and two dimensions.

#### 5.2.1. 1D Burgers' equation

For Burgers' equation in one spatial dimension, we take  $\beta = 1$  and consider the initial condition  $\bar{U} : \Omega \rightarrow \mathbb{R}$

$$\bar{U} : x \mapsto 2(x+1)^2(1-H(x)), \quad (57)$$

where  $H : \mathbb{R} \rightarrow \{0, 1\}$  is the Heaviside function. Our approach only requires a mesh of the reference domain  $\Omega_0 = [-1, 1]$ , which we construct such that an element interface lies at the initial shock location ( $x = 0$ ), i.e., the shock in the initial condition is tracked. The shock tracking solution is computed using a DG discretization on this equispaced mesh with 20 elements of degree  $p = 4, q = 1$  and a DIRK3 temporal discretization with 20 time steps with final time  $T = 1$  (Figure 8).

#### 5.2.2. 2D Burgers' equation

We now consider Burgers' equation in two spatial dimensions. We take  $\Omega_0 = [-1, 1]^2$  as our two-dimensional spatial domain,  $\beta = (1, 0)$  as the flow direction, and  $\bar{U} : \Omega \rightarrow \mathbb{R}$  as the initial condition, defined as

$$\bar{U} : (x_1, x_2) \mapsto \begin{cases} (0.5 - 2(x_2^2 - 0.25)) \left( \frac{4}{3}(x_1 + 0.75) \right) & x \in \Omega_{\square} \\ 0 & \text{elsewhere,} \end{cases} \quad (58)$$

where  $\Omega_{\square} := [-0.75, 0] \times [-0.5, 0.5]$ . The problem is constructed such that the initially straight shock curves over time, which is tracked by the high-order mesh. The shock tracking solution is computed using a DG discretization on a mesh with 128 simplex elements of degree  $p = 2, q = 2$  and a DIRK3 temporal discretization with 40 time steps with final time  $T = 2$  (Figure 9). The mesh smoothing procedure described in Section 4.1 is important here to maintain high-quality elements as the shock moves across the domain.

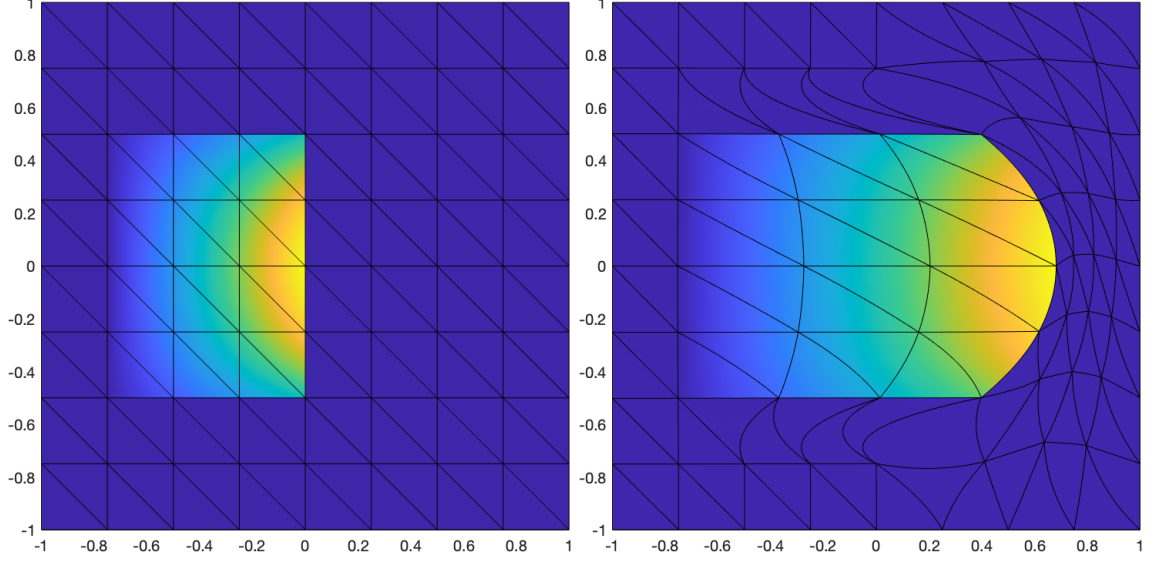
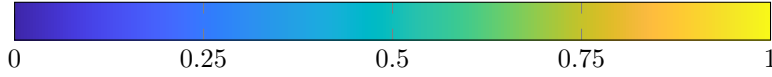


Figure 9: Method of lines solution of two-dimensional, inviscid Burgers' equation with  $p = q = 2$ . Initial condition  $\bar{U}(x)$  (left) and solution at  $T = 2$  (right)



### 5.3. Unsteady, compressible Euler equations

The Euler equations govern the flow of an inviscid, compressible fluid through a domain  $\Omega \subset \mathbb{R}^d$

$$\begin{aligned}
 \frac{\partial}{\partial t} \rho(x, t) + \frac{\partial}{\partial x_j} (\rho(x, t) v_j(x, t)) &= 0 \\
 \frac{\partial}{\partial t} (\rho(x, t) v_i(x, t)) + \frac{\partial}{\partial x_j} (\rho(x, t) v_i(x, t) v_j(x, t) + P(x, t) \delta_{ij}) &= 0 \\
 \frac{\partial}{\partial t} (\rho(x, t) E(x, t)) + \frac{\partial}{\partial x_j} ([\rho(x, t) E(x, t) + P(x, t)] v_j(x, t)) &= 0
 \end{aligned} \tag{59}$$

for all  $x \in \Omega$ ,  $t \in [0, T]$ ,  $i = 1, \dots, d$  and summation is implied over the repeated index  $j = 1, \dots, d$ , where  $\rho : \Omega \times (0, T) \rightarrow \mathbb{R}_+$  is the density of the fluid,  $v_i : \Omega \times (0, T) \rightarrow \mathbb{R}$  for  $i = 1, \dots, d$  is the velocity of the fluid in the  $x_i$  direction, and  $E : \Omega \times (0, T) \rightarrow \mathbb{R}_+$  is the total energy of the fluid, implicitly defined as the solution of (59). For a calorically ideal fluid, the pressure of the fluid,  $P : \Omega \times (0, T) \rightarrow \mathbb{R}_+$ , is related to the energy via the ideal gas law

$$P = (\gamma - 1) \left( \rho E - \frac{\rho v_i v_i}{2} \right), \tag{60}$$

where  $\gamma \in \mathbb{R}_+$  is the ratio of specific heats. By combining the density, momentum, and energy into a vector of conservative variables  $U : \Omega \times [0, T] \rightarrow \mathbb{R}^{d+2}$ , defined as

$$U : (x, t) \mapsto \begin{bmatrix} \rho(x, t) \\ \rho(x, t) v(x, t) \\ \rho(x, t) E(x, t) \end{bmatrix} \tag{61}$$

the Euler equations are a conservation law of the form (1). We investigate the shock tracking framework on two benchmark examples: the Shu-Osher problem and a blast wave problem in 2D.

#### 5.3.1. Shu-Osher Problem

The Shu-Osher problem [36] is a one-dimensional idealization of shock-turbulence interaction where a Mach 3 shock moves into a field with a small sinusoidal density disturbance. The flow domain is  $\Omega_0 =$

$[-4.5, 4.5]$ , and the initial condition is given in terms of the density, velocity, and pressure as

$$\begin{aligned}\rho(x) &= \begin{cases} 3.857143 & x < -4 \\ 1 + 0.2 \sin(5x) & x \geq -4 \end{cases} \\ v(x) &= \begin{cases} 2.629369 & x < -4 \\ 0 & x \geq -4 \end{cases} \\ P(x) &= \begin{cases} 10.3333 & x < -4 \\ 1 & x \geq -4, \end{cases}\end{aligned}\tag{62}$$

and the density, velocity, and pressure are prescribed at  $x = -4.5$  and the velocity is prescribed at  $x = 4.5$  (values can be read from the initial condition). The shock tracking solution is computed using a DG discretization on a mesh with 288 elements of degree  $p = 4$ ,  $q = 1$ , half of which are equispaced to the left of the initial shock location from  $[-4.5, -4]$ , and the other half equispaced from  $[-4, 4.5]$ . The temporal discretization is done by the DIRK3 method with 110 time steps with final time  $T = 1.1$ . The final time is chosen such that waves trailing behind the primary shock do not steepen into shock waves; shock formation will be the subject of future work. In Figure 10, we present the shock tracking solution along with a reference solution computed using a fifth-order WENO method with 200 elements and temporal integration via RK4 with 110 timesteps [36]. The shock tracking solution actually overshoots the reference solution at the formation of the trailing waves, which suggests the reference solution is being overly dissipated by the WENO scheme (*left inset*). The shock is perfectly represented by the aligned mesh in the shock tracking solution compared to the reference (*right inset*).

The SQP solver is used with tolerances  $\epsilon_1 = 10^{-4}$  and  $\epsilon_2 = 10^{-8}$ , which is easily attained at each Runge-Kutta stage and timestep and in very few SQP iterations (Figure 11). We note that the objective function is steadily growing because we are using a fixed amount of resolution to represent an increasingly oscillatory numerical solution. This is not an issue of any other fundamental concern, and can be addressed with adaptive element collapses and refinement, which is straightforward in the one-dimensional case.

The Shu-Osher problem is ideal for implicit shock tracking because it starts off with a well-defined shock that maintains its topology over time and the flow away from the shock is smooth. At present, one could imagine combining this shock tracking approach with a shock capturing method, where strong well-defined shocks could be tracked and weaker shocks which form over time could be captured [24]. Future work will focus on the simulation of the full Shu-Osher problem to additionally track the smaller shocks which form as the trailing waves steepen.

### 5.3.2. Blast Wave

In the final example, we consider a spherical blast wave problem featuring a strong, radially expanding shock. Our problem is inspired by the classic Sedov problem, which is an idealized model of the self-similar evolution of a cylindrical (or spherical) blast wave starting from a large total energy deposited at a single point placed into an otherwise homogenous medium of a uniform ambient density with negligible pressure. The Sedov problem is a workhorse verification test for traditional shock capturing methods since there is an analytical solution [35] available in one-, two-, and three-dimensions for comparison. It is primarily used to test geometrical concerns, such as the ability to track a curved shock and maintain spherical symmetry.

We take  $\Omega = [-1, 1]^2$  as our two-dimensional spatial domain with the initial condition given in terms of the density, velocity, and pressure by a function of the distance from the origin  $r = \sqrt{x_1^2 + x_2^2}$  as

$$\begin{aligned}\rho(r) &= \begin{cases} \frac{5.378}{0.25^2} r^2 & r \leq 0.25 \\ 1 & \text{elsewhere} \end{cases} \\ v(r) &= \begin{cases} \frac{1.304}{0.25} r & r \leq 0.25 \\ 0 & \text{elsewhere} \end{cases} \\ P(r) &= \begin{cases} \frac{0.978}{0.25^2} r^2 + 1 & r \leq 0.25 \\ 10^{-3} & \text{elsewhere} \end{cases}.\end{aligned}\tag{63}$$

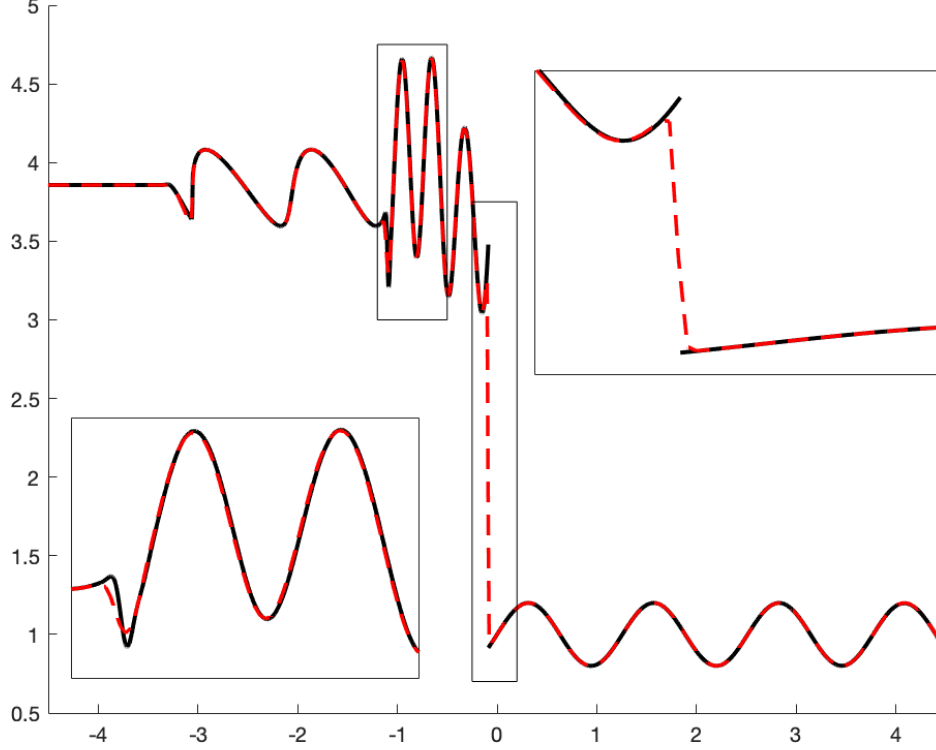


Figure 10: Density at  $T = 1.1$  of Shu-Osher problem for the reference (---) and shock tracking (—) solutions.

Like the other numerical examples considered in this work, the initial condition is constructed such that the shock is exactly meshed. This initial condition is inspired by the solution to the Sedov problem at a time when the primitive variables have already taken on a “bowl-like” structure. The shock tracking solution is computed using a DG discretization on a mesh with 422 simplex elements of degree  $p = 2$ ,  $q = 2$  and a DIRK2 temporal discretization with 140 time steps and final time  $T = 0.14$  (Figure 12). In the shock tracking framework, the ability to track curved shocks accurately while maintaining radial symmetry comes very naturally. Since the initial value for pressure in the ambient region is close to zero and much smaller than the value inside the shock, a slight modification was made to the SQP solver to avoid negative values for energy in the ambient region. After each SQP step, the elements in the ambient region with a negative value for energy are reinitialized with their element-wise average. This helps stabilize the solver in its initial iterations, and it quickly converges from there.

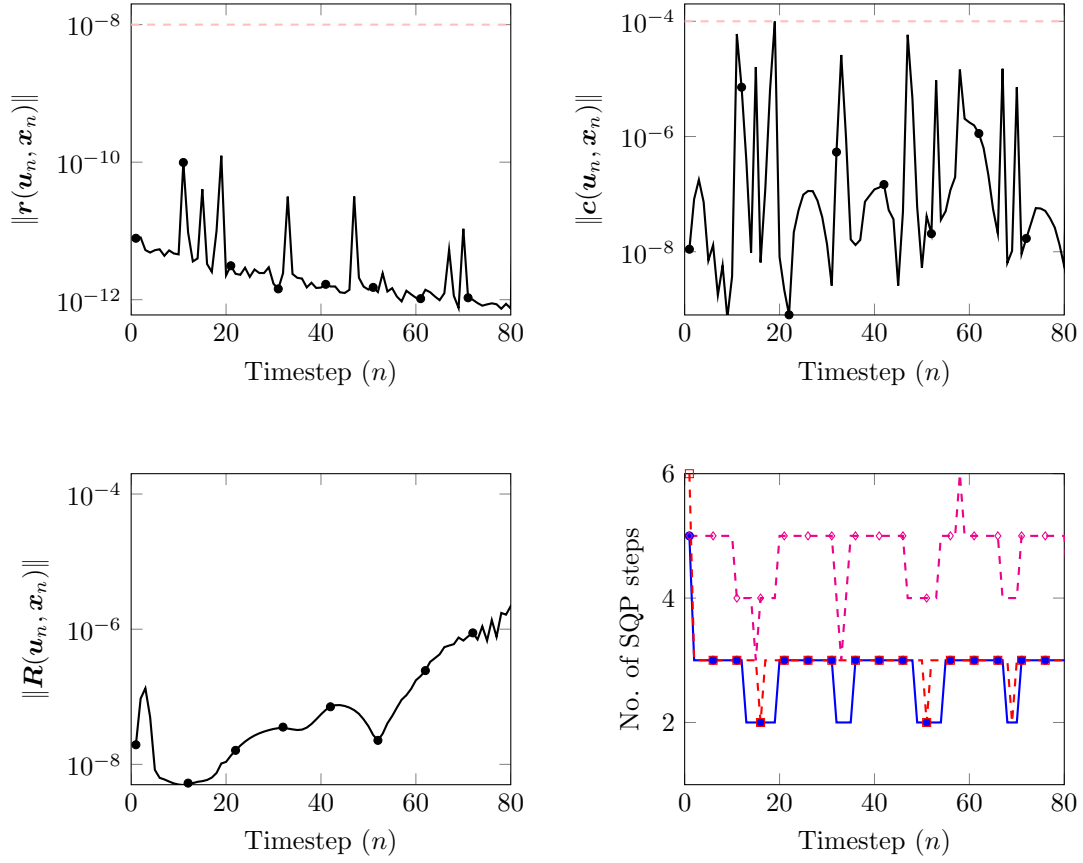


Figure 11: Final converged value of the constraint (*top left*), optimality condition (*top right*), and objective function (*bottom left*) for the solution to the Shu-Osher problem at each timestep ( $\bullet$ ) and the specified tolerances ( $---$ ), and the number of SQP steps needed at each stage of each time step for convergence (*bottom right*); stage 1: ( $\bullet$ ), stage 2 ( $\square$ ), stage 3 ( $\diamond$ ).

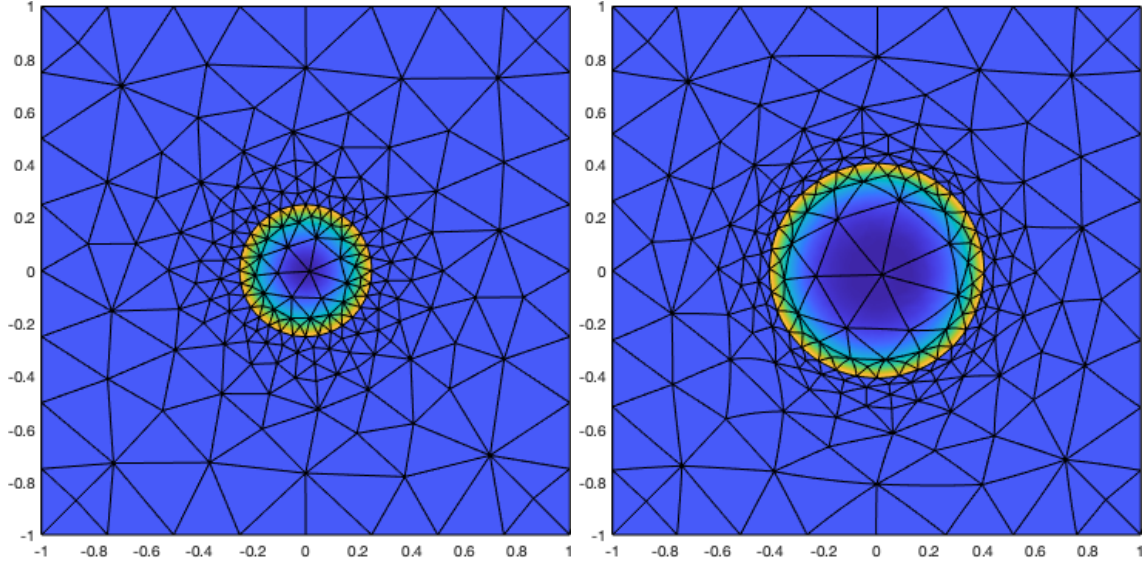


Figure 12: Method of lines solution of two-dimensional blast wave problem with  $p = q = 2$ . Initial condition  $\bar{U}(x)$  (left) and solution at  $T = 0.14$  (right)



## 6. Conclusion and future work

We extend the high-order implicit shock tracking (HOIST) framework for inviscid, steady conservation laws introduced in [45] to the unsteady case by a method of lines discretization via a diagonally implicit Runge-Kutta (DIRK) method. In essence, we are “solving a steady problem at each timestep”, and as such inherit the desirable qualities discussed for the steady case in our previous work, namely a conservative and feature-aligned discretization at each timestep. We demonstrate our framework on a variety of one- and two-dimensional examples, and in particular show that our method is capable of preserving the design order of accuracy of our high-order temporal discretization for both the solution and the shock location, the latter of which is inaccessible to shock capturing methods because they do not maintain a perfect representation of discontinuities. The ability to construct good initial guesses for the optimization problem from information at the previous timestep is key to enable the SQP solver to converge rapidly. This is in contrast to the steady case, where the initial mesh generation and corresponding guess for the solution has to be done independent of the shock location because we lack any *a priori* knowledge. Correspondingly, the steady case requires significant mesh deformation and edge collapses, which needs a more sophisticated line search procedure based on the  $\ell_1$  merit function to achieve convergence. The development of this method of lines approach gives us an additional tool to tackle unsteady problems in addition to the previously developed space-time approach. Generally speaking, the method of lines approach will be more practical and scale better as the size and difficulty of the problem increases. However, it is limited in that it cannot handle colliding shocks (triple points in space-time) without complex mesh operations and solution reinitialization. In these cases, the space-time approach is preferred due to its generality of tracking discontinuities in space-time, which naturally handles triple points.

We see two important avenues of future work in the current setting of time-dependent, inviscid conservation laws. The first issue to consider is shock formation, most commonly illustrated by the time evolution of Burgers’ equation from a smooth initial condition or the steepening of the waves trailing the shock in the Shu-Osher problem. Implicit shock tracking has the potential to cleanly form and subsequently track shocks due to its  $r$ -adaptive behavior and the optimization formulation that *implicitly* tracks shocks and simultaneously resolves the flow; this was shown by the authors of the MDG-ICE method for inviscid and viscous shocks in the space-time setting [10, 26]. In contrast, shock tracking approaches that handle shocks explicitly do not readily show potential to handle shock formation without significant specialization.

Another direction would be the incorporation of topology changes, such as edge flips, refinement and coarsening. In this work, we use a fixed mesh topology as our shock moves across the domain. This limits our ability to accurately resolve the smooth flow in certain areas that only have a fixed amount of grid resolution to represent an increasingly larger portion the spatial domain over time. The issue is somewhat exacerbated by the fact that we are working with very coarse meshes to begin with. This difficulty manifests itself in our numerical experiments, such as in the area immediately trailing the shock of the Shu-Osher problem as well as inside the circular region of the blast wave example as the shock expands radially; this loss of resolution is indicated by the gradual increase in the objective function over time (Figure 11). We emphasize that this is not a fundamental issue and the method performs as expected under the constraint imposed by the fixed topology. However, the incorporation of adaptive mesh coarsening and refinement on curved meshes combined with  $L^2$  error minimizing solution transfer between meshes will unlock the full potential of the method.

Our implicit shock tracking framework has only been introduced and tested on inviscid conservation laws, where perfect discontinuities arise. We expect the framework to be useful for viscous problems with smooth, high-gradient solution features, where the second order viscous terms can be treated using standard techniques [1]. Finally, this paper only considers relatively simple model problems in one- and two- dimensions which feature fairly tame shock motions. Future work will deal with more complex shock phenomena, such as shock-shock and shock-boundary layer interaction.

## Acknowledgments

This material is based upon work supported by the Air Force Office of Scientific Research (AFOSR) under award numbers FA9550-20-1-0236, FA9550-22-1-0002, and FA9550-22-1-0004. The content of this publication does not necessarily reflect the position or policy of any of these supporters, and no official endorsement should be inferred.

## References

- [1] D. N. Arnold, F. Brezzi, B. Cockburn, and L. D. Marini. Unified analysis of discontinuous Galerkin methods for elliptic problems. *SIAM Journal on Numerical Analysis*, 39(5):1749–1779, 2002.
- [2] M. J. Baines, S. J. Leary, and M. E. Hubbard. Multidimensional least squares fluctuation distribution schemes with adaptive mesh movement for steady hyperbolic equations. *SIAM Journal on Scientific Computing*, 23(5):1485–1502, 2002.
- [3] C. E. Baumann and J. T. Oden. A discontinuous  $hp$  finite element method for the Euler and Navier-Stokes equations. *International Journal for Numerical Methods in Fluids*, 31(1):79–95, 1999. Tenth International Conference on Finite Elements in Fluids (Tucson, AZ, 1998).
- [4] J. B. Bell, G. R. Shubin, and J. M. Solomon. Fully implicit shock tracking. *Journal of Computational Physics*, 48(2):223–245, 1982.
- [5] A. Bonfiglioli, R. Paciorri, and L. Campoli. Unsteady shock-fitting for unstructured grids. *International Journal for Numerical Methods in Fluids*, 81(4):245–261, 01 2015.
- [6] A. Burbeau, P. Sagaut, and C.-H. Bruneau. A problem-independent limiter for high-order Runge-Kutta discontinuous Galerkin methods. *Journal of Computational Physics*, 169(1):111–150, 2001.
- [7] M. Ciallella, M. Ricchiuto, R. Paciorri, and A. Bonfiglioli. Extrapolated shock tracking: Bridging shock-fitting and embedded boundary methods. *J. Comput. Phys.*, 412:109440, 2020.
- [8] B. Cockburn and C.-W. Shu. Runge-Kutta discontinuous Galerkin methods for convection-dominated problems. *Journal of Scientific Computing*, 16(3):173–261, 2001.
- [9] A. Corrigan, A. Kercher, and D. Kessler. A moving discontinuous Galerkin finite element method for flows with interfaces. *International Journal for Numerical Methods in Fluids*, 89(9):362–406, 2019.



- [10] A. Corrigan, A. Kercher, and D. Kessler. The moving discontinuous Galerkin method with interface condition enforcement for unsteady three-dimensional flows. In *AIAA Scitech 2019 Forum*, 2019.
- [11] A. Corrigan, A. Kercher, D. Kessler, and D. Wood-Thomas. Convergence of the moving discontinuous galerkin method with interface condition enforcement in the presence of an attached curved shock. In *AIAA Aviation 2019 Forum*, page 3207, 2019.
- [12] L. D’Aquila, B. Helenbrook, and A. Mazaheri. A novel stabilization method for high-order shock fitting with finite element methods. *Journal of Computational Physics*, page 110096, Jan 2021.
- [13] A. Dervieux, D. Leservoisier, P.-L. George, and Y. Coudière. About theoretical and practical impact of mesh adaptation on approximation of functions and PDE solutions. *International Journal for Numerical Methods in Fluids*, 43(5):507–516, 2003. ECCOMAS Computational Fluid Dynamics Conference, Part I (Swansea, 2001).
- [14] K. J. Fidkowski. Output error estimation strategies for discontinuous Galerkin discretizations of unsteady convection-dominated flows. *International Journal for Numerical Methods in Engineering*, 88(12):1297–1322, 2011.
- [15] B. Froehle and P.-O. Persson. Nonlinear elasticity for mesh deformation with high-order discontinuous Galerkin methods for the Navier-Stokes equations on deforming domains. In *Spectral and High Order Methods for Partial Differential Equations ICOSAHOM 2014*, pages 73–85. Springer, 2015.
- [16] A. Gargallo-Peiró, X Roca, J. Peraire, and J. Sarrate. Optimization of a regularized distortion measure to generate curved high-order unstructured tetrahedral meshes. *International Journal for Numerical Methods in Engineering*, 103(5):342–363, 2015.
- [17] A. Gargallo-Peiró, X. Roca, J. Peraire, and J. Sarrate. A distortion measure to validate and generate curved high-order meshes on CAD surfaces with independence of parameterization. *International Journal for Numerical Methods in Engineering*, 106(13):1100–1130, 2016.
- [18] M. Geisenhofer, F. Kummer, and M. Oberlack. An extended discontinuous galerkin method for high-order shock-fitting, 2020.
- [19] J. Glimm, X.-L. Li, Y.-J. Liu, Z.-L. Xu, and N. Zhao. Conservative front tracking with improved accuracy. *SIAM Journal on Numerical Analysis*, 41(5):1926–1947, 2003.
- [20] A. Harten, B. Engquist, S. J. Osher, and S. R. Chakravarthy. Uniformly high-order accurate essentially nonoscillatory schemes. III. *Journal of Computational Physics*, 71(2):231–303, 1987.
- [21] A. Harten and J. M. Hyman. Self adjusting grid methods for one-dimensional hyperbolic conservation laws. *Journal of Computational Physics*, 50(2):235–269, 1983.
- [22] J. Hesthaven and T. Warburton. *Nodal Discontinuous Galerkin Methods: Algorithms, Analysis, and Applications*. Springer Science & Business Media, 2007.
- [23] G.-S. Jiang and C.-W. Shu. Efficient implementation of weighted ENO schemes. *Journal of Computational Physics*, 126(1):202–228, 1996.
- [24] E. Johnsen, J. Larsson, A. V. Bhagatwala, W. H. Cabot, P. Moin, B. J. Olson, P. S. Rawat, S. K. Shankar, B. Sjögreen, H. C. Yee, et al. Assessment of high-resolution methods for numerical simulations of compressible turbulence with shock waves. *Journal of Computational Physics*, 229(4):1213–1237, 2010.
- [25] A. D. Kercher and A. Corrigan. A least-squares formulation of the Moving Discontinuous Galerkin Finite Element Method with Interface Condition Enforcement. *Computers & Mathematics with Applications*, November 2020.

- [26] A. D. Kercher, A. Corrigan, and D. A. Kessler. The moving discontinuous Galerkin finite element method with interface condition enforcement for compressible viscous flows. *International Journal for Numerical Methods in Fluids*, pages 1–30, January 2021.
- [27] X.-D. Liu, S. J. Osher, and T. Chan. Weighted essentially non-oscillatory schemes. *Journal of Computational Physics*, 115(1):200–212, 1994.
- [28] A. Majda. *Compressible fluid flow and systems of conservation laws in several space variables*, volume 53. Springer Science & Business Media, 2012.
- [29] G. Moretti. Thirty-six years of shock fitting. *Computers & Fluids*, 31(4-7):719–723, 2002.
- [30] P.-O. Persson, J. Bonet, and J. Peraire. Discontinuous Galerkin solution of the Navier–Stokes equations on deformable domains. *Computer Methods in Applied Mechanics and Engineering*, 198(17):1585–1595, 2009.
- [31] P.-O. Persson and J. Peraire. Sub-cell shock capturing for discontinuous Galerkin methods. In *44th AIAA Aerospace Sciences Meeting and Exhibit, Reno, Nevada*, 2006. AIAA-2006-0112.
- [32] P. S. Rawat and X. Zhong. On high-order shock-fitting and front-tracking schemes for numerical simulation of shock–disturbance interactions. *Journal of Computational Physics*, 229(19):6744–6780, 2010.
- [33] P.L. Roe. Approximate riemann solvers, parameter vectors, and difference schemes. *Journal of computational physics*, 43(2):357–372, 1981.
- [34] M.D. Salas. *A shock-fitting primer*. CRC Press, 2009.
- [35] L. I. Sedov. *Similarity and dimensional methods in mechanics*. CRC press, 1993.
- [36] C.-W. Shu and S. Osher. Efficient implementation of essentially non-oscillatory shock-capturing schemes, II. In *Upwind and High-Resolution Schemes*, pages 328–374. Springer, 1989.
- [37] G. R. Shubin, A. B. Stephens, and H. M. Glaz. Steady shock tracking and Newton’s method applied to one-dimensional duct flow. *Journal of Computational Physics*, 39(2):364–374, 1981.
- [38] G. R. Shubin, A. B. Stephens, H. M. Glaz, A. B. Wardlaw, and L. B. Hackerman. Steady shock tracking, Newton’s method, and the supersonic blunt body problem. *SIAM Journal on Scientific and Statistical Computing*, 3(2):127–144, 1982.
- [39] J.-Y. Trepanier, M. Paraschivoiu, M. Reggio, and R. Camarero. A conservative shock fitting method on unstructured grids. *Journal of Computational Physics*, 126(2):421–433, 1996.
- [40] J. Van Rosendale. Floating shock fitting via lagrangian adaptive meshes. Technical Report ICASE Report No. 94-89, Institute for Computer Applications in Science and Engineering, 1994.
- [41] Z. J. Wang, K. Fidkowski, R. Abgrall, F. Bassi, D. Caraeni, A. Cary, H. Deconinck, R. Hartmann, K. Hillewaert, H.T. Huynh, et al. High-order CFD methods: current status and perspective. *International Journal for Numerical Methods in Fluids*, 72(8):811–845, 2013.
- [42] J. Yu and J. Hesthaven. A study of several artificial viscosity models within the discontinuous galerkin framework. *Communications In Computational Physics*, 27(5):1309–1343, 2020.
- [43] M. J. Zahr and P.-O. Persson. An optimization-based approach for high-order accurate discretization of conservation laws with discontinuous solutions. *Journal of Computational Physics*, 365:105–134, 2018.
- [44] M. J. Zahr and J. M. Powers. High-order resolution of multidimensional compressible reactive flow using implicit shock tracking. *AIAA Journal*, pages 1–15, 2020.
- [45] M. J. Zahr, A. Shi, and P.-O. Persson. Implicit shock tracking using an optimization-based high-order discontinuous Galerkin method. *Journal of Computational Physics*, 410:109385, June 2020.